HAL open science

Multiphysics modeling of microwave processing for enzyme inactivation in fruit juices

M T K Kubo, S. Curet, P E D Augusto, L. Boillereaux

▶ **To cite this version:**

M T K Kubo, S. Curet, P E D Augusto, L. Boillereaux. Multiphysics modeling of microwave processing for enzyme inactivation in fruit juices. Journal of Food Engineering, 2019, 263, pp.366-379. 10.1016/j.jfoodeng.2019.07.011 . hal-02329848

HAL Id: hal-02329848

https://hal.science/hal-02329848

Submitted on 25 Oct 2021

HAL is a multi-disciplinary open access archive for the deposit and dissemination of scientific research documents, whether they are published or not. The documents may come from teaching and research institutions in France or abroad, or from public or private research centers.

L'archive ouverte pluridisciplinaire **HAL**, est destinée au dépôt et à la diffusion de documents scientifiques de niveau recherche, publiés ou non, émanant des établissements d'enseignement et de recherche français ou étrangers, des laboratoires publics ou privés.

Distributed under a Creative Commons Attribution - NonCommercial 4.0 International License

Version of Record: https://www.sciencedirect.com/science/article/pii/S0260877419302961
Manuscript_78a184085ec71e2020047bc660e0d768

Multiphysics modeling of microwave processing for enzyme inactivation in fruit juices

M. T. K. Kubo [a, b], S. Curet [a,*], P. E. D. Augusto [b,c], L. Boillereaux [a]

[a] GEPEA (UMR 6144 CNRS), ONIRIS, Site de la Géraudière, CS 82225, 44322 Nantes CEDEX 3, France

[b] Department of Agri-food Industry, Food and Nutrition (LAN), Luiz de Queiroz College of Agriculture (ESALQ), University of São Paulo (USP), Piracicaba, SP, Brazil

[c] Food and Nutrition Research Center (NAPAN), University of São Paulo (USP), São Paulo, SP, Brazil

* Corresponding author

E-mail address: sebastien.curet@oniris-nantes.fr (S. Curet)

Abstract

Microwave processing of fruit juice model solution containerized in a cylinder was evaluated by a numerical multiphysics model, aiming to understand the temperature and peroxidase inactivation profiles along processing. In order to rigorously simulate the microwave processing, a finite element model was developed by iteratively coupling electromagnetism, heat transfer, fluid flow and enzyme inactivation. Peroxidase inactivation was determined experimentally, presenting a first-order kinetic behavior ($D_{70°C}$ = 234.377 ± 7.068 s, z = 12.072 ± 0.295 °C, R^2 = 0.97), which was implemented in the simulation. Enzyme inactivation could be well predicted, considering convection currents and spatial temperature distribution within the sample during microwave heating. Experimental results under various combinations of time and temperature were used to validate the results from simulation. Good agreement was obtained in terms of both temperature at the sample center ($R^2 \geq 0.99$) and peroxidase inactivation (R^2 = 0.97). Therefore, the presented results highlight

© 2019 published by Elsevier. This manuscript is made available under the CC BY NC user license
https://creativecommons.org/licenses/by-nc/4.0/

the relevance of a coupled modeling for predicting enzyme inactivation, taking into account the potential presence of cold spots during microwave heating, allowing further process optimization.

Keywords

Microwave heating; Fluid food processing; Finite element modeling; Enzyme inactivation kinetics; Temperature distribution; Fluid flow.

Nomenclature

A/A_0	residual enzyme activity [-]
C_p	heat capacity / specific heat at constant pressure [J kg^{-1} K^{-1}]
D_T	kinetic parameter [s]
e	Euler's number
E	electric field [V m^{-1}]
f	frequency [Hz]
$F_{T_{ref}}$	equivalent holding time at reference temperature [s]
g	gravitational acceleration [m s^{-2}]
h	heat transfer coefficient [W m^{-2} K^{-1}]
H	magnetic field [A m^{-1}]
j	imaginary unit [-]
k	thermal conductivity [W m^{-1} K^{-1}]
L	lethality [-] or sample height [m]
n	normal vector [-]
p	pressure [Pa]
P	power [W]
q	heat flux [W m^{-2}]
Q	heat / power dissipated per unit of volume [W m^{-3}]

r radius [m]

t time [s]

T temperature [°C]

U velocity field [m s^{-1}]

z kinetic parameter [°C]

Greek letters

ε_r' relative dielectric constant, relative electrical permittivity [-]

ε_r'' relative dielectric loss factor [-]

ε_r^* relative complex permittivity [-]

ε_0 permittivity of free space [F m^{-1}]

η viscosity [Pa s]

κ_0 propagation constant within free-space [m^{-1}]

λ wavelength [m]

μ magnetic permeability [H m^{-1}]

μ_0 magnetic permeability of vacuum [H m^{-1}]

ρ density [kg m^{-3}]

σ electrical conductivity [S m^{-1}]

ω pulsation of microwave radiation or angular frequency [rad s^{-1}, Hz]

1. Introduction

Microwave heating has drawn great attention due to its unique characteristics and it has been considered as a promising alternative to conventional heating methods. Microwave heating is primarily based on electromagnetic energy conversion into heat via friction of dipoles and ionic species that try to follow the oscillating electric field. As microwaves can rapidly transfer energy throughout the volume of the material (i.e. volumetric heating), microwave technology can provide faster heating rate, allowing reduced processing time.

Therefore, it can potentially avoid the development of cooked off-flavors, color alteration and degradation of thermosensitive compounds during food processing, better preserving the nutritional and sensory quality of sensitive foods, such as fruits (Guo et al., 2017; Marszałek et al., 2015; Pérez-Grijalva et al., 2018). Also, other important advantages have been attributed to microwave heating, such as the non-requirement of an intermediate heating fluid, lower consumption of water and higher energy efficiency (Ahmed and Ramaswamy, 2007; Zhu et al., 2007b). Therefore, a vast number of microwave applications has been reported in food processing, including pasteurization and blanching of fruit and vegetable-based products (Ahmed and Ramaswamy, 2007; Cañumir et al., 2002; Dorantes-Alvarez and Parada-Dorantes, 2005; Güneş and Bayindirli, 1993; Zhou et al., 2016).

Thermal processing of fruit juices is generally based on the inactivation of heat resistant undesirable enzymes, since the inherent acidity of juices inhibits the development of most pathogens. As peroxidase (POD) is known to have a relatively high heat resistance, whose intensity varies depending on certain conditions, the inactivation of this enzyme is frequently used as an index of processing adequacy (Anese and Sovrano, 2006; Dorantes-Alvarez and Parada-Dorantes, 2005; Stanciuc et al., 2015). Moreover, this enzyme is involved in the oxidation of a wide range of organic and inorganic substrates, resulting in off-flavors and sensory degradation. Microwave heating has been conveniently used to inactivate several enzymes relevant for juice industry, including peroxidase (Benlloch-Tinoco et al., 2013; Latorre et al., 2012; Matsui et al., 2008).

The temperature profile across the product is frequently described as more uniform in microwave heating than in conventional heating methods. Even though, microwave processing still presents the inconvenience of non-uniform heating and uneven temperature distribution (Chandrasekaran et al., 2013; Chen et al., 2014; Vadivambal and Jayas, 2010). Non-uniformity is a limiting factor that restrain the broad application of microwave technology in the industry. The non-uniform temperature distribution not only affects the energy efficiency during processing (due to overheating of hot spots) but also raises the issue of food quality and safety. As thermal effects remain the main lethal mechanism known in

microwave processing, undesirable enzymes and microorganisms may not be inactivated in the cold spots within the product during a non-uniform heating.

Therefore, a study of temperature distribution and heat transfer is needed to understand and optimize the process. Microwave heating depends on interactions of several factors and involves complex multiphysics phenomena. In the case of heating of liquids, the complexity is even greater because of buoyancy-driven flow. Thus, the evaluation of the processing only by experimental means can be difficult, time consuming and inviable, hence the need for the use of computational tools.

Numerical modeling has been employed to simulate the microwave processing in different systems and apparatus, aiming to evaluate, optimize and scale-up the process. Many studies in the literature have reported numerical simulations of microwave heating in solid materials and gels (Chen et al., 2014; Curet et al., 2008; Hamoud-Agha et al., 2014; Lin et al., 1995; Romano et al., 2005). Simulations dealing with microwave heating of liquid and pumpable foods in continuous flow (Salvi et al., 2011; Tuta and Palazoglu, 2017; Zhu et al., 2007b, 2007a) and in containers (Chatterjee et al., 2007; Cherbański and Rudniak, 2013; Zhang et al., 2000) can also be found.

Numerical simulation of microwave heating of liquids, especially when enclosed within a container, is more challenging than the one of solids, due to the presence of natural convection phenomena. Consequently, this problem requires solving the electromagnetism, heat transfer and fluid dynamics equations, simultaneously. Some studies have made use of simplifications for modeling microwave processing of fluids, such as using an approach of Lambert's law for the heat source (Chatterjee et al., 2007; Datta, 2001) and considering a two-dimensional study (Ayappa et al., 1994; Klinbun and Rattanadecho, 2012; Ratanadecho et al., 2002). However, these approaches are limited. For instance, fluid convection is three-dimensional in nature, which limits the conclusions based on 2D models. Moreover, Lambert's law approach provides less accurate results for modeling the heat generation, thus the Maxwell's equations need to be solved to exactly describe electromagnetism, especially in thin and cylindrical samples (Oliveira and Franca, 2002; Yang and Gunasekaran, 2004).

The model complexity is also increased when both fluid dynamics and inactivation of enzyme are considered during a microwave heating process.

With the recent computational advances and continuous software improvements, more numerical investigations on coupled 3D multiphysics microwave heating models dedicated to liquids have been reported (Cherbański and Rudniak, 2013; Choi et al., 2015; Salvi et al., 2011; Tuta and Palazoglu, 2017; Yeong et al., 2017). Nevertheless, to our knowledge, there is a lack of studies on microwave heating combined with enzyme inactivation, highlighting both experimental and numerical data, dedicated to packaged liquid foods.

In order to evaluate the processing and predict the enzyme inactivation by microwave heating, a reliable numerical model need to be developed taking into account the presence of cold spots and the interactions of microwave heating, flow fields and local temperature distributions to the inactivation kinetic. Therefore, the aim of this study was to evaluate numerically and experimentally the application of microwave heating on a model fruit juice, focusing on the inactivation of peroxidase (POD).

2. Material and methods

The present work was developed in three parts, using a fruit juice model solution as the sample to be processed. In the first part, this solution was submitted to thermal processing at different conditions of time and temperature and the kinetic parameters of enzyme inactivation was calculated. Then, in the second part, the juice model solution was processed by microwave and the residual enzyme activities were measured. Finally, the experimental conditions of the microwave processing (from second part) as well as the obtained kinetic model of enzyme inactivation (from first part) were used to develop the simulation model. The experimental results of enzyme inactivation by microwaves and measured temperatures were later applied to validate the multiphysics model.

165 ### *2.1. Sample preparation*

166 This work was carried out using the fruit juice model solution proposed by Kubo et al.
167 (2018b) and composed of sucrose (Synth, Brazil), citric acid (Synth, Brazil), horseradish
168 peroxidase (POD type X, P6140 - 25 KU, Sigma-Aldrich Co., USA) and distilled water. The
169 juice model solution was defined and prepared in order to mimic a simplified real fruit juice
170 composition. Through this approach, a better control of the sample properties and
171 reproducibility of results were possible. The soluble solids content, initial enzymatic activity
172 and pH of the model solution were 10 °Brix, 4 U mL^{-1} and 3.8, respectively. Fresh fruit juice
173 model solution was prepared daily, just before each processing.

174

175 ### *2.2. Kinetic modeling of enzyme inactivation*

176 #### *2.2.1. Thermal processing*

177 To evaluate the enzyme inactivation kinetic, conventional thermal processing of fruit
178 juice model solution was performed in such a way as to be possible to consider the sample
179 temperature as homogeneous across the product during processing. Thus, thermal histories
180 could be properly assessed together with the residual activities of peroxidase.

181 The thermal processing was conducted by placing 4 mL aliquots of the model juice in
182 glass tubes with small diameter (10 mm) and thin walls (0.6 mm). The tubes were positioned
183 in a holder inside a thermostatic water bath (Dubnoff MA 095/CFRE, Marconi, Brazil) with
184 orbital shaking at 150 rpm. The thermal processing was carried out at seven process
185 temperatures (T_P = 60, 62, 64, 66, 68, 70, 72 °C) and six process times (heating + holding
186 times) for each T_P.

187 After the desirable holding time, the samples were quickly cooled in an ice-water bath
188 until the temperature reached 5 °C. The temperature history of each sample was monitored
189 using T-thermocouples fixed in the center of the tube through a cap and connected to a data
190 logger (Almemo 2890-9, Ahlborn, Germany), with sampling rate of 1 per second. All
191 experiments were performed in triplicate.

192

193 ***2.2.2. Enzyme activity assay***

194 The POD activity was determined according to the method described by Augusto et
195 al. (2015). The enzyme activity assays were performed using pyrogallol as the substrate, at
196 room temperature and pH 6.0. The desired pH was obtained using a McIlvaine's buffer
197 solution, which was prepared by combining determined volumes of 0.1 mol L^{-1} citric acid
198 (Synth, Brazil) solution and 0.2 mol L^{-1} sodium phosphate dibasic (Synth, Brazil) solution
199 (McIlvaine, 1921).

200 In each assay, 160 µL of sample, 2.25 mL of McIlvaine's buffer solution at pH 6.0 and
201 320 µL of 5% (m/v) pyrogallol solution (Sigma-Aldrich Co., UK) were mixed in a quartz
202 cuvette with a 1-cm light path. The mixture of all reactants was used as a reference solution
203 (0.000 absorbance). Then, 160 µL of 0.147 mol L^{-1} hydrogen peroxide solution (Synth, Brazil)
204 was added to start the reaction. The increase of absorbance at 420 nm was monitored for
205 2 min using an UV-Vis spectrophotometer (UV-1240, Shimadzu, Japan).

206 The enzyme activity was calculated based on the variation of absorbance using a
207 generalized reduced gradient algorithm implemented in the 'Solver' tool of software Excel
208 2016 (Microsoft, USA), as described by Kubo et al. (2018b). The enzyme activity of each
209 thermally processed tube was evaluated at least in duplicate. The residual activity (A/A_0)
210 was calculated by the ratio of the enzyme activity after the process (A) to the initial activity
211 (A_0) before thermal processing.

212

213 ***2.2.3. Enzyme inactivation kinetics model***

214 Based on previous studies, the first-order kinetic model was selected to describe the
215 thermal inactivation kinetic of POD in the juice model solution (Kubo et al., 2018b). It
216 considers only one enzymatic portion to be inactivated and can be written as follows:

$$log\left(\frac{A}{A_0}\right) = -\frac{t}{D_T} \quad (1)$$

where D_T value is the time required for a 90% reduction of enzyme activity at a specific temperature T. The effect of temperature on the D_T value is expressed as a z value and it can be described as:

$$log\left(\frac{D_T}{D_{Tref}}\right) = \frac{T_{ref} - T}{z} \tag{2}$$

During conventional thermal processing, the samples were processed in a non-isothermal way, i.e. the heating and cooling of the sample were not instantaneous. However, the Eq.(1) is only suitable under isothermal conditions. Thus, in order to take into account the actual contribution of the temperature history to the inactivation, the concepts of lethality (L) and equivalent holding time ($F_{T_{ref}}$) were needed.

The accumulated lethality at any location in the sample can be obtained by integrating the effect of temperature profile on enzyme inactivation during the whole processing. The accumulated lethality can be expressed as the equivalent holding time (Eq.(3)), which corresponds to the processing time at a reference temperature (T_{ref}) that results in a lethality equivalent to the actual and non-isothermal processing.

$$F_{T_{ref}} = \int_0^t L(t)\,dt = \int_0^t 10^{\left(\frac{T(t)-T_{ref}}{z}\right)}\,dt \tag{3}$$

Therefore, to determine the POD inactivation kinetic considering the non-isothermal temperature profile, the predicted residual activities by the first-order kinetic were calculated from the numerical evaluation of the Eq.(4), which is a combination of Eq.(1) and Eq.(3). The values of $F_{T_{ref}}$ were calculated by using the trapezoidal method (Murasaki-Aliberti et al., 2009). Due to the small diameter and thin walls of the tube, the low viscosity of the sample and the vigorous agitation in the water bath, the temperature was assumed to be homogeneous throughout the sample over the whole conventional thermal processing.

The parameters of the kinetic model (D_T and z values) were iteratively adjusted by a non-linear estimation procedure implemented in the 'Solver' tool of software Excel 2016 (Microsoft, USA), minimizing the sum of squared errors (SSE) between experimental and

predicted residual enzymatic activities. Uncertainty estimates were calculated by the macro 'SolverAid' (De Levie, 2004). The minimized SSE and the coefficient of determination R^2 were used to report the fit criteria of the model.

$$\frac{A_t}{A_0} = 10^{\left(-\frac{F_{T_{ref}}}{D_{T_{ref}}}\right)} \quad (4)$$

2.3. Microwave processing

2.3.1. Microwave system

Microwave processing was performed in a microwave apparatus, which supplied waves in the fundamental single-mode, denoted TE_{10}, operating at a frequency of 2.45 GHz. The experimental apparatus was basically composed of: a microwave generator (magnetron type), a waveguide, an applicator and a water load. A schematic representation of the microwave system, indicating its main components, is presented in Figure 1.

The generator (GMP03KSM, Sairem, France) was connected to the waveguide through a coaxial cable connected to a WR340 waveguide transition. Microwave energy was transmitted along the z-direction of the rectangular waveguide (cross-section 86 mm X 43 mm) made of brass. To ensure that a minimal amount of microwave was reflected back to the sample and magnetron, a water load was fixed at the bottom end of the guide, located about 40 cm distance from the applicator. This water load consisted of a quartz tube through which water at 15 °C from a thermostatic bath circulated at a flow rate of around 820 mL min^{-1}.

The applicator was positioned in the middle of the waveguide. Since both of them had the same rectangular transversal section, the applicator can be considered as a continuation of the waveguide. It is in the applicator that the sample was placed to be heated. The experimental temperature of the sample was measured and recorded by a fiber optic sensor connected to a data logger (Reflex-4, Neoptix, Canada).

In order to monitor the microwave processing along the time, the generator and the waveguide were instrumented by power sensors that were connected to a data logger (Datalog 20, AOIP, France). Knowledge of actual power values is important not only for control and monitoring of the process but also as an input data in the model for microwave heating simulations – once this value changes over the processing time. During the transmission of the microwave energy from the generator to the waveguide, some losses in the transmission lines can occur along the path, such as losses in the coaxial cable, intermediate connectors and waveguide transition. Therefore, a directional coupler (VT26WHHC40NC, Vector Telecom, Australia) connected to a power meter (HX2462A, Techniwave, France) was placed after the applicator. The maximum actual incident power was measured and found to be equal to 105 W within an empty waveguide terminated with a water load. This value was then implemented in the simulation model as the maximum input power.

2.3.1. Experimental setup

A support block made of extruded polystyrene with 60 mm in height was placed inside the applicator. The block, filling the cross-section of the waveguide, serves as a support for a small tube of 10.13 mm external diameter, 7.93 mm internal diameter and 35.80 mm height. This tube containing an aliquot of 1.2 mL of sample was placed in the center of the block, where the amplitude of electric field was maximum (TE_{10} mode). A cylindrical polystyrene cap was used to close the tube, to limit possible sample evaporation and to ensure the position of the fiber optic sensor to measure the temperature at the geometrical center of the sample. A schematic diagram of the applicator is shown in Figure 2A.

Preliminary tests were performed to compare the transmitted power through the empty applicator and through the applicator containing the polystyrene block and plastic tube (without sample). The same values of power were obtained in both cases, indicating these materials do not absorb microwave energy (very low loss tangent of polystyrene).

291 Experiments were performed at seven central holding temperatures (T_H = 60, 62, 64,
292 66, 68, 70, 72 °C) and four holding times for each T_H. For the sake of simplicity, in this work,
293 the term "central holding temperature" refers to the target temperature for the holding phase
294 measured at the geometrical center of the product using a fiber optic sensor. A PID
295 temperature controller (Eurotherm 2408/2404, UK) was used to maintain T_H at its expected
296 setpoint during the appropriate residence time by acting on the incident power. After each
297 treatment, the sample was removed from the applicator and rapidly cooled in an ice bath until
298 5 °C.

299 All experiments were performed in triplicate. Enzyme activity of the samples was
300 determined shortly after the processing and the residual activity was calculated.

301

302 ## *2.4. Model development*

303 The first step in the model development was the definition of the model geometry,
304 computational domain and appropriate assumptions. Then, the properties of the materials
305 and the heat transfer coefficient were obtained. All this information was implemented in the
306 iterative numerical model, which coupled the RF module, the CFD module and the Heat
307 Transfer module. The enzyme inactivation kinetic was also implemented in the model. A
308 more detailed description of the numerical model development and its main steps, including
309 the initial and boundary conditions, the considerations made and the governing equations
310 related to each module, is presented as follows. Finally, to ensure the validity of all the
311 assumptions, an experimental validation of the developed model was performed, comparing
312 the predicted values with the results from experiments at 28 conditions of holding time and
313 temperature.

314

315 ### *2.4.1. Model geometry: description and simplification*

316 The model geometry was based on the apparatus used for microwave processing of
317 the juice solution and described above. However, some modifications and considerations

were needed. Since 3D models require considerable computational effort, it is highly recommendable to simplify the geometry of the problem whenever possible.

In the present case, the fact of using a TE_{10} mode waveguide allowed an interesting simplification. For an empty rectangular waveguide filled with air, in the plane xy, the electric field has only one component (E_y), whose maximum amplitude is located in the center of the waveguide and in turn, in the center of the sample, as shown in Figure 2B. Also, the distribution of the electric field is uniform along b (y-axis), varying only along a (x-axis) and direction of wave propagation (z-axis). Therefore, instead of considering the whole geometry, it was possible to model only ¼ of the waveguide and sample, which allowed a substantial reduction of computational resources and time required for simulations. For that, some boundary conditions at the walls were considered as described later (Eq.(14) and Eq.(16)), ensuring the symmetry (Curet et al., 2014).

Another important simplification was made in the model. It consisted of not consider neither the plastic tube, nor the support block, nor the cap in the computational domain. For the fluid flow resolution, a no slip condition was applied at the wall. In this way, the sample was assumed to be surrounded by air. Preliminary tests showed that none of these neglected items absorb microwave energy, indicating that this modification does not affect the electromagnetic field modeling. However, it affects the modeling of heat transfer, since the sample surface loses heat to the tube, the support, the cap and the surrounding air during processing. Therefore, the knowledge of heat transfer around the sample was needed and it was obtained through the determination of a global heat transfer coefficient, which was estimated experimentally as described later. Figure 3 illustrates the final simplified geometry considered in the computational domain.

2.4.2. General assumptions and considerations

In order to model the microwave heating of the fruit juice model solution, the following assumptions were made:

- The product was considered as homogeneous and isotropic (i.e. it had the same physical properties independently of direction);
- The initial temperature of the solution was uniform (Equation 22);
- There was no mass transfer and evaporation;
- The external environment temperature was constant and fixed to 20 °C (Equation 23);
- The sample was initially at rest (i.e., $U_x = U_y = U_z = 0$);
- The fluid movement was considered as a "weakly compressible flow" (term from the software settings option), in which the sample properties are function of temperature but not of pressure (COMSOL, 2018);
- The walls of the rectangular waveguide were considered as perfect electric conductors;
- Sample was considered as non-magnetic;
- The product was surrounded by a medium with zero dielectric losses (air), thus, heat transfer was not spatially solved within the surrounding medium (air). However, natural convection to the air was considered as a boundary condition with the global heat transfer coefficient determined experimentally;
- Polystyrene support and plastic tube did not interact with the electromagnetic field;
- The fiber optic sensor is considered sufficiently thin to neglect its influence on the fluid motion;
- At the end of the waveguide, there was no wave reflection (perfectly matched water load).

2.4.3. Thermophysical properties of the fruit juice model solution

All the thermophysical properties of the fruit juice model solution were implemented in the model in the form of equations as a function of temperature. Thermal conductivity (k), heat capacity (C_p) and viscosity (η), data were obtained from literature. Density (ρ) and dielectric properties (ε_r', ε_r'') were obtained experimentally using the fruit juice model solution.

372 The main components of the fruit juice model solution are water and sucrose. Thus, it
373 is reasonable to consider that the thermal properties and viscosity of the 10 °Brix juice are
374 close to that of a 10% (w/w) sucrose solution. In this way, data on thermal conductivity, heat
375 capacity and viscosity at different temperatures were obtained from literature and fitted by
376 equations, which are presented in Table 1.

377 Density was measured by weighing the volume of model juice contained in standard
378 volumetric pycnometers previously calibrated with distilled water at each temperature (20 –
379 80 °C) (Figura and Teixeira, 2007). Water density data obtained from Haynes (2014) were
380 used as reference. Measurements were carried out in triplicate.

381 Since many materials undergo thermal expansion, i.e. increase in volume when
382 heated, the density of a liquid usually decreases with temperature. As expected, the density
383 of the fruit juice model solution decreased with increasing temperature (Figure 4A). Data was
384 fitted to a quadratic equation. By performing a comparison with the literature, the
385 experimental values of the juice model solution density were close to the values found for 10
386 °Brix sucrose solution by Honig (1953) and Mathlouthi and Reiser (1995). This suggests that
387 data for sucrose solution could also be used in the simulation model, as it was done for the
388 other properties mentioned above.

389 Dielectric properties determinations of the model fruit juice were carried out using an
390 open-ended coaxial line probe system with a Dielectric Probe Kit 85070E (high temperature
391 configuration) connected to an Electronic Calibration Module 85092-60010 and a Network
392 Analyzer E5062A (Agilent Technologies, Malaysia). Dielectric constant ($\varepsilon_r^{'}$) and loss factor
393 ($\varepsilon_r^{''}$) were measured at 2.45 GHz in the temperature range of 20 – 80 °C, as described by
394 Kubo et al. (2018a). The experiments were performed in triplicate. Ten measurements were
395 done for each repetition and temperature evaluated.

396 The obtained dielectric properties of the model juice solution at 2.45 GHz are
397 presented in Figure 4B. The observed trend is in accordance with that reported for fruit juices
398 and other beverages (Franco et al., 2015; Kubo et al., 2018a; Zhu et al., 2012). As the other

properties, both dielectric constant and loss factor data were adjusted to polynomial equations (Table 1).

It is noteworthy that temperature-dependence of the dielectric and thermophysical properties was considered. These properties have an important role in the governing equations of the numerical model. Briefly, the modeling involves: the calculation of heat generation (at first, based on properties at the initial temperature), the estimation of temperature profile and distribution by solving the heat transfer and fluid flow equations, the re-computation of heat generation and electric field using properties based on the previous obtained temperatures (Datta, 2001; Salvi et al., 2011). The use of approximated values by considering the thermophysical properties as independent of temperature may lead to less accurate results.

Therefore, all the equations used to describe the properties of the fruit juice model solution as a function of temperature are presented in Table 1, including all the digits considered in the model.

2.4.4. Global heat transfer coefficient

During processing, there are some heat losses from the sample surface to its surrounding via convection and conduction. Thus, in order to model this heat flux taking into account all the involved materials and geometries, an experimental approach was performed and the global heat transfer coefficient (h_{global}) was estimated via Lumped Capacitance Method (Incropera et al., 2007).

In the experiment, a solid yellow brass cylinder with the same dimensions of the plastic tube was heated until around 70 °C or cooled until around 5 °C. Experiments of cooling and heating were carried out in triplicate. Therefore, considering six experiment repetitions, the mean value of h_{global} was 6.48 W m^{-2} K^{-1}. The suitability of this value was successfully verified through a numerical study, evaluating the heat flux and temperature profile (data not shown).

2.4.5. Modeling of electromagnetism

The modeling of microwave interactions with dielectric materials is governed by the classical Maxwell's equations, which were computed within both waveguide and sample. Using the RF module and the Electromagnetic Waves, Frequency Domain as the physics-based modeling interface in the COMSOL Multiphysics® software, the microwave heating generation was deduced from the electromagnetic field distribution. Electromagnetic Waves, Frequency Domain is a predefined physics interface frequently employed to model microwave devices, in which the following governing equation for electric field propagation is solved:

$$\nabla \times \mu_r^{-1}(\nabla \times \vec{E}) - \kappa_0^2 \left(\varepsilon_r' - \frac{j\sigma}{\omega\varepsilon_0}\right)\vec{E} = 0 \tag{5}$$

where the propagation constant within free-space (κ_0), the electrical conductivity of a dielectric sample (σ), the pulsation of microwave radiation (ω) and the complex permittivity (ε^*) are defined as follows, respectively:

$$\kappa_0 = \omega\sqrt{\varepsilon_0\mu_0} \tag{6}$$

$$\sigma = \omega\varepsilon_0\varepsilon_r'' \tag{7}$$

$$\omega = 2\pi f \tag{8}$$

$$\varepsilon^* = \varepsilon' - j\varepsilon'' = \varepsilon_0(\varepsilon_r' - j\varepsilon_r'') \tag{9}$$

Based on the model geometry previously described and depicted in Figure 2 and Figure 3, the main associated initial and boundary conditions were:

- $\vec{E} = \vec{0}$ at $t = 0, \forall xyz$ (10)
- $E_{in} = E_0 \cos\left(\frac{\pi x}{a}\right) = \sqrt{4\, Z_{TE} \frac{P_{in}}{ab}} \cos\left(\frac{\pi x}{a}\right)$ at $z = +\infty, \forall xy$ (11)
- $\vec{n} \times (\vec{H}_{air} - \vec{H}_{sample}) = \vec{0}$ at $z = -\frac{L}{2}, z = \frac{L}{2}, \forall xy \in [0, r]$ (12)
- $\vec{n} \times (\vec{H}_{air} - \vec{H}_{sample}) = \vec{0}$ at $x, y = r, \forall z \in [-\frac{L}{2}, \frac{L}{2}]$ (13)

- $\vec{n} \times \vec{H} = \vec{0}$ at $x = 0, \forall zy, \forall t > 0$ (14)
- $\vec{n} \times \vec{E} = \vec{0}$ at $x = \frac{a}{2}, \forall zy, \forall t > 0$ (15)
- $\vec{n} \times \vec{E} = \vec{0}$ at $y = 0, \forall zx, \forall t > 0$ (16)
- $\vec{n} \times \vec{E} = \vec{0}$ at $y = -\frac{b}{2}, \forall zx, \forall t > 0$ (17)

Due to the simplification of the computational domain, some conditions were particularly needed for the modeling of electromagnetism. The conditions of perfect electric conductor (Eq.(16)) and of perfect magnetic wall (Eq.(14)) were considered in the walls where the geometry was "cut", as indicated in gray in Figure 3. These boundary conditions were implemented to consider the symmetry at the center of the waveguide.

2.4.6. Modeling of heat transfer

Heat transfer was solved within the liquid sample using the Heat Transfer module of COMSOL Multiphysics® software. It was based on the general heat equation with an energy source term to calculate the temperature distribution due to conduction and convection with heat generation:

$$\rho C_p \frac{\partial T}{\partial t} + \rho C_p \vec{U} \cdot \nabla T - \nabla \cdot \vec{q} = Q_{gen} \quad (18)$$

$$\text{where } \vec{q} = k \cdot \nabla T \quad (19)$$

where ρ is the density, C_p is the specific heat capacity, $\vec{U}$ is the velocity vector and k is the thermal conductivity of the material. The heat generation due to microwave (Q_{gen}) was computed from the local electric field (E_{local}) strength at any point of the cylindrical sample:

$$Q_{gen} = \frac{1}{2} \omega \varepsilon_0 \varepsilon_r'' \, |E_{local}|^2 \quad (20)$$

The term Q_{gen} is defined as the amount of heat dissipated per unit of volume within a dielectric material. In other words, it represents the heat source responsible for the temperature rise in the product. During the experiments of microwave processing, a PID temperature controller was used to modulate the incident power in order to maintain the

temperature at specific values of T_H. Thus, the variation of incident power of each experiment along the processing time was monitored and applied to modulate the heat source in the numerical model.

The heat losses due to convection/conduction phenomena around the sample were also calculated, taking into consideration the model geometry simplification (Section 2.4.1.) and the global heat transfer coefficient (h_{global}) previously described (Section 2.4.4.):

$$q_{global} = h_{global}(T_\infty - T) \tag{21}$$

The main associated initial and boundary conditions for heat transfer modeling were:

- $T = T_{initial}$ at $t = 0, \forall x\ \forall y\ \forall z$ (22)
- $T_\infty = 20\ °C,\ \forall t \geq 0$ (23)
- $-n \cdot \vec{q} = q_{global}$ at $x, y = r, \forall z\ \in \left[-\frac{L}{2}, \frac{L}{2}\right],\ \forall t \geq 0$ (24)
- $-n \cdot \vec{q} = q_{global}$ at $z = -\frac{L}{2}, z = \frac{L}{2}, \forall xy\ \in [0, r],\ \forall t \geq 0$ (25)

2.4.7. Modeling of fluid flow

In computational simulation software, such as COMSOL Multiphysics®, the solution of fluid motion equations can be based on three types of flow: incompressible, compressible and weakly compressible. Liquids are much less compressible than gases. Then, for liquids under certain conditions, the flow can be considered as incompressible. It means that the density is assumed to be constant and continuity equation can be simplified. Generally, in these situations, the Boussinesq approximation is also considered. Nevertheless, in some cases, this approximation is not ideal and an intermediate scenario can be assumed for more accuracy. The flow can be considered as weakly compressible, in which density is dependent on temperature (COMSOL, 2018). In this way, fluid flow was modeled considering a laminar flow of a Newtonian weakly compressible fluid using the CFD module and Laminar Flow interface of COMSOL Multiphysics® software.

The Navier-Stokes equation governs the fluid flow, taking into account the inertial forces, pressure forces, viscous forces and gravitational force applied to the fluid. In this case, it can be represented as follows:

$$\rho\frac{\partial\vec{U}}{\partial t}+\rho(\vec{U}\cdot\nabla)\vec{U}=\nabla\cdot\left[-pI+\eta\left(\nabla\vec{U}+(\nabla\vec{U})^{T}\right)-\frac{2}{3}\eta(\nabla\cdot\vec{U})I\right]-\rho\vec{g} \tag{26}$$

where p is the fluid pressure, I is the identity matrix and η is the viscosity and $\vec{g}$ is the gravitational acceleration.

Besides the Navier-Stokes equation, the continuity equation was also solved:

$$\frac{\partial\rho}{\partial t}+\nabla\cdot(\rho\vec{U})=0 \tag{27}$$

While the Navier-Stokes equation represents the conservation of momentum, the continuity equation represents the conservation of mass.

The main associated initial and boundary conditions for fluid flow modeling were:

- $\vec{U}=\vec{0}$ at the sample side and bottom walls (no slip condition), $\forall t\geq 0$ (28)
- $U_x=0;\ U_y=0;\ U_z=0$ at $t=0$ (29)
- $p=p_{atm}+\rho g\left(z-\frac{L}{2}\right)$, $\forall z$ with $-\frac{L}{2}\leq z\leq+\frac{L}{2}$ (30)

2.4.8. Modeling of enzyme inactivation

The enzyme inactivation during microwave processing was calculated by integrating the POD inactivation kinetic model (previously described in section 2.2.3.) in the simulation. However, since the temperature distribution within the sample was non-uniform during the microwave processing, the equivalent holding time ($F_{T_{ref}}$) was computed taking into account not only the time but also the space, as shown below:

$$F_{T_{ref}}=\int^{t}\iiint^{xyz}L(t,x,y,z)\,dt\,dxdydz=\int^{t}\iiint^{xyz}10^{\left(\frac{T(t,x,y,z)-T_{ref}}{z}\right)}dt\,dxdydz \tag{31}$$

From the equation above, the temperature effect within the whole 3D geometry of the sample throughout processing time was considered. Using the obtained value of

accumulated lethality, the global enzyme inactivation was calculated according to Eq.(4). In this way, the predicted value of residual enzyme activity could be compared with the value obtained experimentally and, thus, the model could be validated.

2.4.9. Computational details and numerical procedure

Based on a Finite Element Method, the numerical study was performed using the software COMSOL Multiphysics® 5.3a in a Dell Precision T7910 workstation (2x processors Intel Xeon at 2.5GHz, 256 GB of RAM, Windows 8.1 Professional, 64 bits).

The user-defined mesh consisted of 113.679 tetrahedral elements in the total domain and of 76.468 elements in the sample domain. The maximum element sizes were 0.4 mm for the sample and 4.32 mm for the rest of the domain. This very fine mesh within the sample was necessary in order to capture efficiently the fluid flow coupled with the heat generation due to microwaves. For the fluid flow resolution, a boundary layer mesh was built along the sample walls in order to compute accurate solutions and resolve the velocity gradients that generally arise at the surfaces where wall conditions are considered.

The simulation of microwave processing was run in two steps. Firstly, a stationary study solving only the fluid flow was performed. This stationary study was performed to initialize the velocity field within the fluid by considering a constant initial temperature of 20 °C. Then, in the second step, a complete time-dependent study was performed using the Backward Differentiation Formula (BDF) solver with default settings and initial time step of 10^{-8} s. Electromagnetism (frequency domain), heat transfer and fluid flow equations were considered and coupled together. The integration related to enzyme inactivation was performed during the post-processing stage. The total time required for each simulation run was around 2 – 4 days.

522 ***2.4.10. Model validation***

523 The simulated time intervals and the values of input power varied according to each
524 microwave treatment (i.e. each time-temperature combination) and its repetition. Thus, these
525 values were implemented in the simulation model based on the experimental values. For the
526 model validation, the simulated temperature profile and the predicted residual enzyme
527 activity were compared with the experimental data from the respective microwave treatment.

528

529 **3. Results and discussion**

530 ***3.1. Enzyme inactivation kinetics***

531 All the residual enzymatic activities as well as their corresponding thermal histories
532 from all the thermal processing repetitions were employed to obtain the inactivation kinetics
533 model. Since there is no specific isothermal holding time, any temperature within the range of
534 study (60 –72 °C) could be used as a reference temperature (Tajchakavit and Ramaswamy,
535 1997). The reference temperature T_{ref} was then set to 70 °C.

536 Considering the non-isothermal profile of the processing, the accumulated lethality at
537 70 °C was calculated and, due to the observed behavior, the inactivation data were fitted to a
538 first-order kinetic model. Adjusted kinetic parameters and fit criteria obtained through iterative
539 non-linear estimation procedure are shown in Table 2. The predicted inactivation curve and
540 experimental residual activities as a function of $F_{T_{ref}}$ for 70 °C are presented in Figure 5A. A
541 parity chart comparing the predicted data and the experimental values obtained after thermal
542 processing at different T_P is shown in Figure 5B. By observing the fit criteria and the figure,
543 the first-order kinetic model showed good suitability to fit POD inactivation data under the
544 evaluated conditions.

545 Therefore, the data of Table 2 were used in the numerical simulation, as follows.

546

547 ### *3.2. Enzyme inactivation by microwave processing*

548 The microwave processing experiments were performed at seven T_H (60, 62, 64, 66,
549 68, 70, 72 °C) and four holding times for each T_H, totaling 28 treatments. During microwave
550 processing, a temperature controller was used to modulate the incident microwave power in
551 order to maintain the temperature at the desired T_H. Such values of incident power were
552 normalized based on the maximum actual incident power measured within the empty
553 waveguide using a power meter (105 W) and were later implemented in the simulation
554 model. Examples of the temperature profile along the time for the treatments at 60 °C/8 min
555 and 72 °C/3 min are shown in Figure 6A and its respective variation of the normalized
556 incident power is shown in Figure 6B.

557 For a numerical evaluation of the incident energy within the waveguide, the integral of
558 the incident power versus time curves was calculated using the software MATLAB® 7.10 (The
559 MathWorks, Inc., USA). The results of energy as well as the residual peroxidase activities
560 assessed after microwave processing are presented in the Table 3 (mean values, n = 3).

561 As expected, at a determined T_H, the longer the processes, the higher the inactivation
562 degree and the larger the amount of energy required. It is interesting to observe that only a
563 portion of the microwave energy is absorbed by the sample due to its small size. Actually, the
564 main part of this energy is absorbed within the water load at the bottom end of the
565 waveguide, ensuring a minimal microwave reflection towards back the sample and
566 magnetron. The values of residual peroxidase activities were later compared to predicted
567 values and employed to validate the simulation model described below.

568

569 ### *3.3. Numerical simulation of microwave processing*

570 From the simulation, 3D-temperature distributions within the sample along the
571 processing time were predicted. Figure 7 illustrates some examples of temperature
572 distributions during two microwave treatments: 60 °C/1 min and 72 °C/3 min (T_H/holding
573 time), at the middle and the end of the respective processing times.

Uneven temperature patterns were clearly distinguished, mainly in the beginning and middle of the processing time. The bottom side of the sample presented lower temperatures, which is probably result of the combination of resonance phenomena and fluid flow patterns within the small sample. It can be observed that the differences of temperature at hot and cold zones were about 8 – 12 °C. These differences are critical, since undesirable enzymes and microorganisms may not be sufficiently inactivated, raising the issue of product quality and safety and highlighting the importance of the numerical evaluation presented in this work.

Over the time, the temperature differences within the sample tend to slightly decrease, as observed at the end of the processing times. The temperature distribution has tendency to present less heterogeneity when compared to early stages of heating, which can be explained by the presence of fluid flow and the changing values of dielectric properties and penetration depth as a function of time-temperature. In fact, fluid flow contributes to homogeneity by mixing the sample, having an important effect on temperature distribution as further discussed (Section 3.4).

Dielectric properties are temperature-dependent (Figure 4B). As time goes on, at 2.45 GHz, temperature increases and loss factor decreases, leading to a reduced energy absorption. Thus, in the regions where the local temperatures are higher, the heating presents smaller heating rates, contributing to a more uniform temperature distribution (Franco et al., 2017; Zhang et al., 2000). Similar observation of reduced temperature gradient was reported for water heated by microwave in a rectangular container (Zhang et al., 2000).

Besides, the microwave power intensity decays as the wave propagates through the sample, which is expressed by the penetration depth - defined as the distance at which the incident power is reduced to 1/e of its value at the surface of the material (Sosa-Morales et al., 2010). Although the penetration depth is a concept that may not be directly applied for moving fluids, a qualitative conjecture can be discussed. At 2.45 GHz, the calculated values of penetration depth increased with temperature: the penetration depths of microwaves into

602 the model fruit juice, considering the medium static and homogeneous, would range from
603 11.3 mm (at 20 °C) to 38.9 mm (at 80 °C). At lower temperatures (< 60 °C) the penetration
604 depth would be smaller than the liquid height (24.3 mm). Thus, since the incident
605 microwaves propagate through the sample from the top surface, it may help to explain the
606 colder temperatures at the bottom region at shorter processing times, when both temperature
607 and penetration depth were smaller. However, it is important to highlight once again that the
608 obtained temperature profile is a consequence of simultaneous different phenomena,
609 including fluid flow, electric field distribution and microwave penetration depth.

610 In addition to the temperature, the simulation also provided information about the fluid
611 flow and velocity field within the sample. The modeling of the fluid motion was mainly the
612 result of the coupling between fluid flow and heat transfer equations. The temperature rise
613 during the process promotes natural convection currents due to the differences of fluid
614 density at different temperatures.

615 Figure 8 presents an example from the treatment at 66 °C/5 min, in which
616 temperature and velocity of fluid flow are shown. It can be noticed that velocity values are
617 higher at the upper region of the sample, where the temperatures are also higher – which
618 can also help to explain the more homogeneous temperature in this part. Similar patterns of
619 temperature and velocity were reported for microwave heating of water containerized in a
620 round-bottomed flask of 0.08 m diameter (Yeong et al., 2017).

621 In the example of microwave processing at 66 °C/5 min (Figure 8), the maximum
622 velocity was around 1.8 mm s^{-1}, which is quite significant considering the size of the sample.
623 However, lower magnitudes of the predicted velocities were found at the bottom portion of
624 the sample. As a result, the microwave induced natural convection motion was not enough to
625 avoid the presence of cold zones and temperature non-uniformity over the entire sample
626 volume, confirming that non-uniform microwave heating is an issue not only for solid but also
627 liquid foods.

628

629 ### *3.4. Model validation: temperature profile and enzyme inactivation*

630 Predicted values of the temperature profile at the geometric center of the sample
631 were compared with the experimental values. Although 28 microwave treatments were
632 simulated, only the results for the microwave processing at retention time and T_H
633 combinations of: 60 °C/8 min, 62 °C/6 min, 64 °C/7 min, 66 °C/5 min, 68 °C/6 min,
634 70 °C/3 min and 72 °C/3 min, are presented in Figure 9. Complete presentation of the
635 temperature profiles of all microwave treatments can be found as Supplementary material.

636 Overall, a very good agreement in terms of temperature was obtained in every
637 simulation of each microwave treatment, especially at intermediate processing temperatures
638 - T_H (66 – 68 °C). At other T_H, slight deviations between predicted and experimental
639 temperatures, either upwards or downwards, can be observed. These minor differences may
640 be due to the consideration of a single and constant global heat transfer coefficient between
641 sample and surrounding, which might actually be variable along the process.

642 Predicted values of the residual peroxidase activity after microwave processing were
643 compared with the experimental values. As shown in Figure10A, a quite good agreement
644 was obtained between both predicted and experimental values. The inactivation is closely
645 dependent on spatial temperature distribution throughout the microwave processing.
646 Therefore, considering the satisfactory results, the approach of integrating the lethality at
647 each point within the sample volume at each instant of time and calculating the accumulated
648 lethality was suitable and valid.

649 Besides, these results demonstrated the successful employment of the inactivation
650 kinetic model from conventional (water bath) to microwave heating. In other words, it
651 demonstrates that the most important effect on peroxidase inactivation by microwave is the
652 thermal effect.

653 As a complementary part of the model validation, a verification of the importance of
654 fluid flow coupling on the quality of the predicted results was performed – once this
655 simplification is sometimes considered in order to save computational effort. For this

656 purpose, two simulations of the treatment at 66 °C/5 min were compared: one solving and
657 coupling the fluid flow equations, and another neglecting the fluid flow.

658 As expected, a great difference was observed in relation to the simulation run time.
659 While the complete model took 87 h, the model without fluid flow needed only around 20 h to
660 be solved. Nevertheless, by comparing both situations, remarkable differences can be
661 observed in the temperature profile, with a poor correlation between the experimental and
662 simulated values when convection is neglected. To illustrate this difference, the temperature
663 distribution within the sample at the processing time of 675 s was simulated using a model
664 with (Figure 11A) and without (Figure 11B) coupling of the fluid flow equations. In the
665 simulated processing without considering fluid flow, the temperature distribution is clearly
666 more uneven, with hot zones around the center of the sample and two cold zones located in
667 the top and bottom side. This heating pattern can be explained by the so-called focusing
668 effect of microwaves, typically reported for spherical and cylindrical solid materials (Zhang
669 and Datta, 2005). Therefore, this result highlights that fluid flow indeed plays a significant role
670 on the spatial temperature distribution during microwave heating.

671 Due to the different temperature distribution, the global enzyme inactivation was
672 also different, as it can be observed Figure 10B. When fluid flow was not solved, less
673 inactivation occurred since more cold zones were found within the sample (Figure 11B).
674 Thus, in view of all the presented results, one can conclude that to obtain a reliable model of
675 microwave heating of liquid and enzyme inactivation, the resolution of the fluid flow equations
676 is strictly necessary, even if greater computational effort is required.

677 Concluding, given the good agreement between experimental and numerical results
678 of both temperature and enzyme inactivation, one can consider the simulation model as
679 successfully validated. Hence, the coupling of electromagnetism, heat transfer, fluid flow and
680 enzyme inactivation kinetics was appropriate. Therefore, the developed simulation model can
681 be employed as a tool to design and optimize microwave processing of fruit juices and other
682 liquid foods, aiming adequate inactivation even with the presence of induced convection flow
683 and the occurrence of cold zones within the sample during heating.

4. Conclusions

By using a Finite Element method, a multiphysics model to simulate a batch microwave heating of a fruit juice model solution and predict peroxidase inactivation was proposed. Dielectric and thermophysical properties were considered as a function of temperature in the model. Governing equations of electromagnetism, heat transfer and fluid flow were coupled and solved. The first-order peroxidase inactivation kinetics, resulting from experiments with conventional heating, was incorporated in the numerical simulations.

The results showed the presence of convection currents and uneven temperature distribution within the sample. Thus, the approach of accumulated lethality was used and combined with fluid flow and local temperature predictions. The lethal effect of temperature evolution over the whole geometrical volume, taking into account the presence of cold zones, was numerically integrated to estimate the enzyme inactivation.

Microwave treatments of the model fruit juice solution at several combinations of time and temperature were performed. Information on temperature profile at the geometric center of the sample as well as peroxidase inactivation data were obtained. The experimental results were used to validate the numerical model. Overall, quite good agreement was observed.

As a perspective, the developed model can be adapted to simulate other operating conditions encountered in the industry. For example, the model could be used to evaluate a microwave processing of a liquid food at 915 MHz. Also, other inactivation kinetic models could be implemented, depending on the target of the processing.

In conclusion, this work presents an interesting tool to evaluate the uniformity of the process and its effectiveness on the inactivation, which can further be used to design and optimize processes in order to obtain ideal food quality and safety.

Acknowledgements

The authors are grateful to the National Council for Scientific and Technological Development – CNPq (Brazil) for funding the PhD scholarship of M.T.K. Kubo (233347/2014-3), the project 401004/2014–7 and the productivity grant of P.E.D. Augusto (306557/2017-7).

References

Ahmed, J., Ramaswamy, H.S., 2007. Microwave pasteurization and sterilization of foods, in: Rahman, M.S. (Ed.), Handbook of Food Preservation. CRC Press, Boca Raton, FL, pp. 691–711.

Anese, M., Sovrano, S., 2006. Kinetics of thermal inactivation of tomato lipoxygenase. Food Chem. 95, 131–137. https://doi.org/10.1016/j.foodchem.2004.12.026

Augusto, P.E.D., Ibarz, R., Garvín, A., Ibarz, A., 2015. Peroxidase (POD) and Polyphenol Oxidase (PPO) Photo-Inactivation in a Coconut Water Model Solution Using Ultraviolet (UV). Food Res. Int. 74, 151–159. https://doi.org/10.1016/j.foodres.2015.04.046

Ayappa, K.G., Brandon, S., Derby, J.J., Davis, H.T., Davis, E.A., 1994. Microwave driven convection in a square cavity. AIChE J. 40, 1268–1272. https://doi.org/10.1002/aic.690400718

Benlloch-Tinoco, M., Igual, M., Rodrigo, D., Martínez-Navarrete, N., 2013. Comparison of microwaves and conventional thermal treatment on enzymes activity and antioxidant capacity of kiwifruit puree. Innov. Food Sci. Emerg. Technol. 19, 166–172. https://doi.org/10.1016/j.ifset.2013.05.007

Cañumir, J. a, Celis, J.E., de Bruijn, J., Vidal, L. V, 2002. Pasteurisation of Apple Juice by Using Microwaves. Leb. und-Technologie 35, 389–392. https://doi.org/10.1006/fstl.2001.0865

Chandrasekaran, S., Ramanathan, S., Basak, T., 2013. Microwave Food Processing — A review. Food Res. Int. 52, 243–261. https://doi.org/10.1016/j.foodres.2013.02.033

Chatterjee, S., Basak, T., Das, S.K., 2007. Microwave driven convection in a rotating

cylindrical cavity: A numerical study. J. Food Eng. 79, 1269–1279. https://doi.org/10.1016/j.jfoodeng.2006.04.039

Chen, J., Pitchai, K., Birla, S., Negahban, M., Jones, D., Subbiah, J., 2014. Heat and mass transport during microwave heating of mashed potato in domestic oven--model development, validation, and sensitivity analysis. J. Food Sci. 79, E1991-2004. https://doi.org/10.1111/1750-3841.12636

Cherbański, R., Rudniak, L., 2013. Modelling of microwave heating of water in a monomode applicator- Influence of operating conditions. Int. J. Therm. Sci. 74, 214–229. https://doi.org/10.1016/j.ijthermalsci.2013.07.001

Choi, W., Lee, S.H., Kim, C.T., Jun, S., 2015. A finite element method based flow and heat transfer model of continuous flow microwave and ohmic combination heating for particulate foods. J. Food Eng. 149, 159–170. https://doi.org/10.1016/j.jfoodeng.2014.10.016

Curet, S., Rouaud, O., Boillereaux, L., 2014. Estimation of Dielectric Properties of Food Materials During Microwave Tempering and Heating. Food Bioprocess Technol. 7, 371–384. https://doi.org/10.1007/s11947-013-1061-4

Curet, S., Rouaud, O., Boillereaux, L., 2008. Microwave tempering and heating in a single-mode cavity: Numerical and experimental investigations. Chem. Eng. Process. Process Intensif. 47, 1656–1665. https://doi.org/10.1016/j.cep.2007.09.011

Datta, A.K., 2001. Mathematical Modeling of Microwave Processing of Foods : An Overview, in: Irudayaraj, J. (Ed.), New York. Marcel Dekker, New York.

De Levie, R., 2004. Advanced Excel for scientific data analysis. Oxford University Press, New York.

Dorantes-Alvarez, L., Parada-Dorantes, L., 2005. Blanching using microwave processing, in: Schubert, H., Regier, M. (Eds.), The Microwave Processing of Foods. CRC Press, Boca Raton, FL, pp. 153–173.

Figura, L.O., Teixeira, A.A., 2007. Food physics: physical properties – measurement and applications, 1st ed. Springer-Verlag Berlin Heidelberg, Berlin.

https://doi.org/10.1007/978-3-540-34194-9

Franco, A.P., Tadini, C.C., Andrey, J., Gut, W., Patrícia, A., Tadini, C.C., Wilhelms, J.A., 2017. Predicting the dielectric behavior of orange and other citrus fruit juices at 915 and 2450 MHz. Int. J. Food Prop. 20, 1468–1488. https://doi.org/10.1080/10942912.2017.1347674

Franco, A.P., Yamamoto, L.Y., Tadini, C.C., Gut, J. a. W., 2015. Dielectric properties of green coconut water relevant to microwave processing: Effect of temperature and field frequency. J. Food Eng. 155, 69–78. https://doi.org/10.1016/j.jfoodeng.2015.01.011

Güneş, B., Bayindirli, A., 1993. Peroxidase and lipoxygenase inactivation during blanching of green beans, green peas and carrots. LWT - Food Sci. Technol. https://doi.org/10.1006/fstl.1993.1080

Guo, Q., Sun, D.W., Cheng, J.H., Han, Z., 2017. Microwave processing techniques and their recent applications in the food industry. Trends Food Sci. Technol. 67, 236–247. https://doi.org/10.1016/j.tifs.2017.07.007

Hamoud-Agha, M.M., Curet, S., Simonin, H., Boillereaux, L., 2014. Holding time effect on microwave inactivation of Escherichia coli K12: Experimental and numerical investigations. J. Food Eng. 143, 102–113. https://doi.org/10.1016/j.jfoodeng.2014.06.043

Haynes, W.M. (Ed.), 2014. CRC Handbook of chemistry and physics, 95th ed. CRC Press, Boca Raton.

Honig, P., 1953. Principles of sugar technology. Elsevier, Amsterdam.

Incropera, F.P., DeWitt, D.P., Bergman, T.L., Lavine, A.S., 2007. Fundamentals of heat and mass transfer, 6th ed. John Wiley & Sons, New York.

Klinbun, W., Rattanadecho, P., 2012. Analysis of microwave induced natural convection in a single mode cavity (Influence of sample volume , placement , and microwave power level). Appl. Math. Model. 36, 813–828. https://doi.org/10.1016/j.apm.2011.07.003

Kubo, M.T.K., Augusto, P.E.D., Cristianini, M., 2013. Effect of high pressure homogenization (HPH) on the physical stability of tomato juice. Food Res. Int. 51, 170–179.

https://doi.org/10.1016/j.foodres.2012.12.004

Kubo, M.T.K., Curet, S., Augusto, P.E.D., Boillereaux, L., 2018a. Artificial Neural Network for prediction of dielectric properties relevant to microwave processing of fruit juice. J. Food Process Eng. e12815.

Kubo, M.T.K., Rojas, M.L., Curet, S., Boillereaux, L., Augusto, P.E.D., 2018b. Peroxidase inactivation kinetics is affected by the addition of calcium chloride in fruit beverages. LWT - Food Sci. Technol. 89, 610–616. https://doi.org/10.1016/j.lwt.2017.11.045

Latorre, M.E., Bonelli, P.R., Rojas, A.M., Gerschenson, L.N., 2012. Microwave inactivation of red beet (Beta vulgaris L. var. conditiva) peroxidase and polyphenoloxidase and the effect of radiation on vegetable tissue quality. J. Food Eng. 109, 676–684. https://doi.org/10.1016/j.jfoodeng.2011.11.026

Lin, Y.E., Anantheswaran, R.C., Puri, V.M., 1995. Finite element analysis of microwave heating of solid foods. J. Food Eng. 25, 85–112.

Marszałek, K., Mitek, M., Skąpska, S., 2015. Effect of Continuous Flow Microwave and Conventional Heating on the Bioactive Compounds, Colour, Enzymes Activity, Microbial and Sensory Quality of Strawberry Purée. Food Bioprocess Technol. 8, 1864–1876. https://doi.org/10.1007/s11947-015-1543-7

Mathlouthi, M., Reiser, P. (Eds.), 1995. Sucrose: properties and applications. Springer US.

Matsui, K.N., Gut, J.A.W., de Oliveira, P.V., Tadini, C.C., 2008. Inactivation kinetics of polyphenol oxidase and peroxidase in green coconut water by microwave processing. J. Food Eng. 88, 169–176. https://doi.org/10.1016/j.jfoodeng.2008.02.003

McIlvaine, T.C., 1921. A buffer solution for colorimetric comparison. J. Biol. Chem. 183–186.

Murasaki-Aliberti, N.D.C., Da Silva, R.M.S., Gut, J. a W., Tadini, C.C., 2009. Thermal inactivation of polyphenoloxidase and peroxidase in green coconut (Cocos nucifera) water. Int. J. Food Sci. Technol. 44, 2662–2668. https://doi.org/10.1111/j.1365-2621.2009.02100.x

Oliveira, M.E.C., Franca, a. S., 2002. Microwave heating of foodstuffs. J. Food Eng. 53, 347–359. https://doi.org/10.1016/S0260-8774(01)00176-5

Pérez-Grijalva, B., Herrera-Sotero, M., Mora-Escobedo, R., Zebadúa-García, J.C., Silva-Hernández, E., Oliart-Ros, R., Pérez-Cruz, C., Guzmán-Gerónimo, R., 2018. Effect of microwaves and ultrasound on bioactive compounds and microbiological quality of blackberry juice. LWT - Food Sci. Technol. 87, 47–53. https://doi.org/10.1016/j.lwt.2017.08.059

Ratanadecho, P., Aoki, K., Akahori, M., 2002. A numerical and experimental investigation of the modeling of microwave heating for liquid layers using a rectangular wave guide (effects of natural convection and dielectric properties). Appl. Math. Model. 26, 449–472. https://doi.org/10.1016/S0307-904X(01)00046-4

Romano, V.R., Marra, F., Tammaro, U., 2005. Modelling of microwave heating of foodstuff: study on the influence of sample dimensions with a FEM approach. J. Food Eng. 71, 233–241. https://doi.org/10.1016/j.jfoodeng.2004.11.036

Salvi, D., Boldor, D., Aita, G.M., Sabliov, C.M., 2011. COMSOL Multiphysics model for continuous flow microwave heating of liquids. J. Food Eng. 104, 422–429. https://doi.org/10.1016/j.jfoodeng.2011.01.005

Sosa-Morales, M.E., Valerio-Junco, L., López-Malo, a., García, H.S., 2010. Dielectric properties of foods: Reported data in the 21st Century and their potential applications. LWT - Food Sci. Technol. 43, 1169–1179. https://doi.org/10.1016/j.lwt.2010.03.017

Stanciuc, N., Aprodu, I., Ioniţa, E., Bahrim, G., Râpeanu, G., 2015. Exploring the process-structure-function relationship of horseradish peroxidase through investigation of pH- and heat induced conformational changes. Spectrochim. Acta - Part A Mol. Biomol. Spectrosc. 147, 43–50. https://doi.org/10.1016/j.saa.2015.03.023

Tajchakavit, S., Ramaswamy, H.S., 1997. Continuous-Flow Microwave Inactivation Kinetics of Pectin Methyl Esterase in Orange Juice. J. Food Process. Preserv. 21, 365–378. https://doi.org/10.1111/j.1745-4549.1997.tb00790.x

Tuta, S., Palazoglu, T.K., 2017. Finite element modeling of continuous-flow microwave heating of fluid foods and experimental validation. J. Food Eng. 192, 79–92. https://doi.org/10.1016/j.jfoodeng.2016.08.003

Vadivambal, R., Jayas, D.S., 2010. Non-uniform Temperature Distribution During Microwave Heating of Food Materials—A Review. Food Bioprocess Technol. 3, 161–171. https://doi.org/10.1007/s11947-008-0136-0

Yang, H.W., Gunasekaran, S., 2004. Comparison of temperature distribution in model food cylinders based on Maxwell's equations and Lambert's law during pulsed microwave heating. J. Food Eng. 64, 445–453. https://doi.org/10.1016/j.jfoodeng.2003.08.016

Yeong, S.P., Law, M.C., Vincent Lee, C.C., Chan, Y.S., 2017. Modelling batch microwave heating of water. IOP Conf. Ser. Mater. Sci. Eng. 217. https://doi.org/10.1088/1757-899X/217/1/012035

Zhang, H., Datta, A.K., 2005. Heating concentrations of microwaves in spherical and cylindrical foods: Part Two: In a cavity. Food Bioprod. Process. 83, 14–24. https://doi.org/10.1205/fbp.04047

Zhang, Q., Jackson, T.H., Ungan, A., 2000. Numerical modeling of microwave induced natural convection. Int. J. Heat Mass Transf. 43, 2141–2154. https://doi.org/10.1016/S0017-9310(99)00281-1

Zhou, L., Tey, C.Y., Bingol, G., Bi, J., 2016. Effect of microwave treatment on enzyme inactivation and quality change of defatted avocado puree during storage. Innov. Food Sci. Emerg. Technol. 37, 61–67. https://doi.org/10.1016/j.ifset.2016.08.002

Zhu, J., Kuznetsov, a. V., Sandeep, K.P., 2007a. Mathematical modeling of continuous flow microwave heating of liquids (effects of dielectric properties and design parameters). Int. J. Therm. Sci. 46, 328–341. https://doi.org/10.1016/j.ijthermalsci.2006.06.005

Zhu, J., Kuznetsov, A. V., Sandeep, K.P., 2007b. Numerical simulation of forced convection in a duct subjected to microwave heating. Heat Mass Transf. und Stoffuebertragung 43, 255–264. https://doi.org/10.1007/s00231-006-0105-y

Zhu, X., Guo, W., Wu, X., 2012. Frequency- and temperature-dependent dielectric properties of fruit juices associated with pasteurization by dielectric heating. J. Food Eng. 109, 258–266. https://doi.org/10.1016/j.jfoodeng.2011.10.005

Figure 1. Schematic representation of the microwave system and its main components: 1) microwave generator, 2) energy control panel, 3) computer, 4) data logger for power and temperature records, 5) data logger for fiber optic sensors, 6) coaxial cable, 7) coaxial isolator, 8) WR340 waveguide transition, 9) rectangular waveguide, 10) applicator, 11) power meter, 12) water load, 13) water bath, 14) power control, 15) temperature controller.

Figure 2. (A) Schematic diagram of the applicator and experimental setup for the microwave processing of fruit juice model solution. (B) Views of the arrangement of the sample, plastic tube, polystyrene cap and support inside the TE_{10} mode rectangular waveguide, where a = 86 mm, b = 43 mm, L = 24.3 mm. Electric field distribution within an empty TE_{10} waveguide in the plane xy is illustrated by dotted arrows in green.

Figure 3. Model design simplification and computational domain, where a = 86 mm (x-axis), b = 43 mm (y-axis), L = 24.3 mm (z-axis) and r = 3.965 mm.

Figure 4. (A) Density and (B) dielectric constant and loss factor at 2.45 GHz of the fruit juice model solution as a function of temperature. Vertical bars indicate the standard deviation.

Figure 5. (A) Residual peroxidase activity (A/A_0) as a function of the equivalent time ($F_{70°C}$, considering 70 °C as the reference temperature), where green square dots are the experimental values, the vertical bars are the standard deviation and the black dotted curve is the adjusted first-order model. (B) Parity chart between the values predicted by the model and the experimental data obtained after thermal treatment at different processing temperatures (T_P).

Figure 6. (A) Temperature profiles at the center of the fruit juice model solution and (B) normalized incident power along the microwave processing at the following holding temperatures and times: 60 °C for 8 min and 72 °C for 3 min.

Figure 7. Temperature distribution within the sample at the middle and the end of processing times of two microwave heating conditions: (A) 60 °C/1 min and (B) 72 °C/3 min.

Figure 8. Distribution of temperature (contour plots) and velocity of fluid flow (volume plots) within the fruit juice model solution during the microwave treatment of 66 °C/5 min at the processing time of 675 s.

Figure 9. Predicted and experimental temperature profile at the center of the sample during the following microwave treatments: (A) 60 °C/8 min, (B) 62 °C/6 min, (C) 64 °C/7 min, (D) 66 °C/5 min, (E) 68 °C/6 min, (F) 70 °C/3 min and (G) 72 °C/3 min.

Figure 10. (A) Parity plots comparing the predicted and experimental residual peroxidase activity in fruit juice model solution after 28 different microwave treatments. (B) Parity plots comparing the predicted, considering or not fluid flow, and experimental residual peroxidase activity after the microwave treatment at 66 °C/5 min.

Figure 11. Temperature (T) distribution within the juice model solution and electric field (E) distribution, both at time of 675 s of a microwave treatment at 66 °C/5 min based on simulations considering fluid flow (A) and neglecting fluid flow (B).

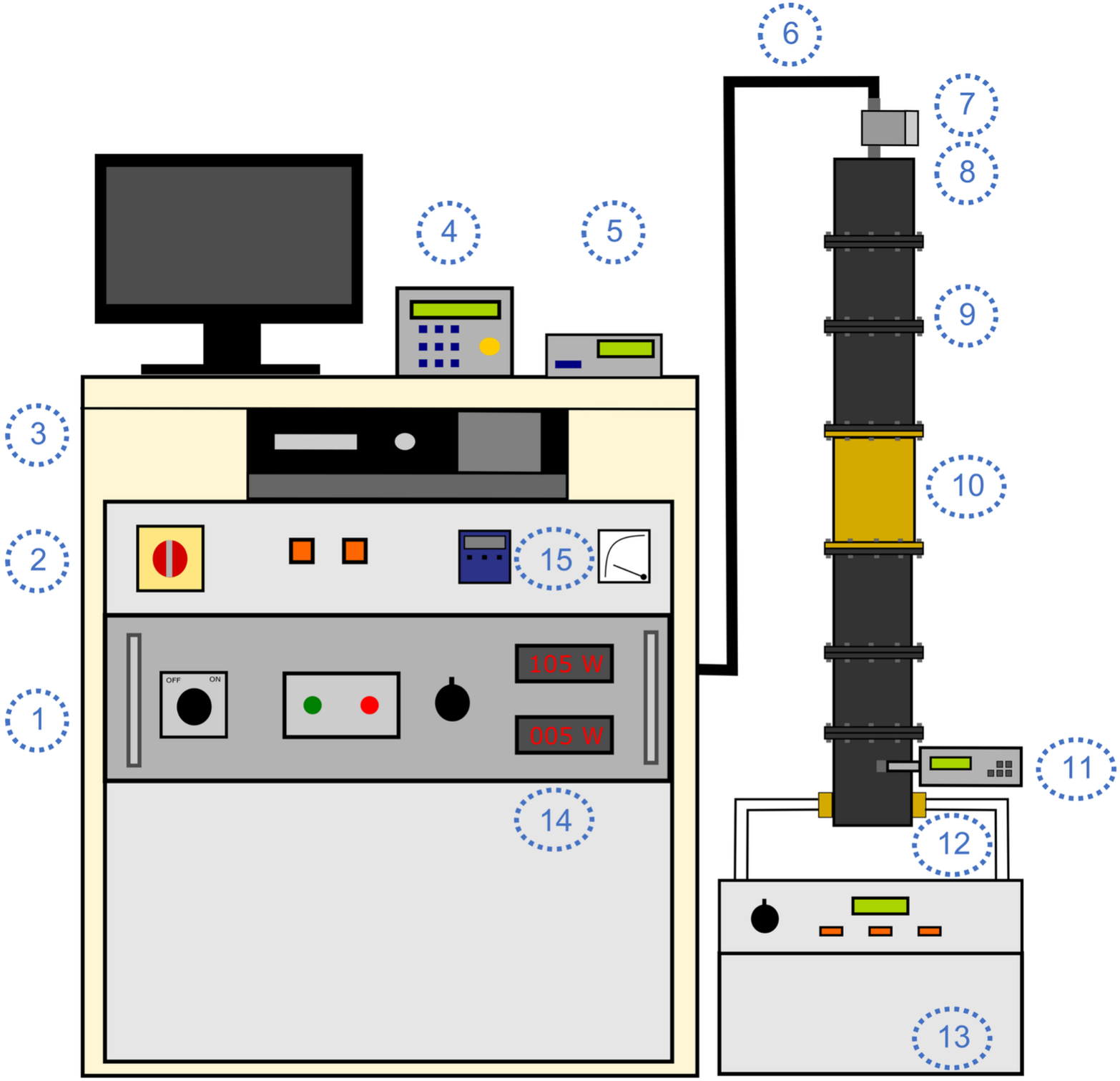

Figure 1. Schematic representation of the microwave system and its main components: 1) microwave generator, 2) energy control panel, 3) computer, 4) data logger for power and temperature records, 5) data logger for fiber optic sensors, 6) coaxial cable, 7) coaxial isolator, 8) WR340 waveguide transition, 9) rectangular waveguide, 10) applicator, 11) power meter, 12) water load, 13) water bath, 14) power control, 15) temperature controller.

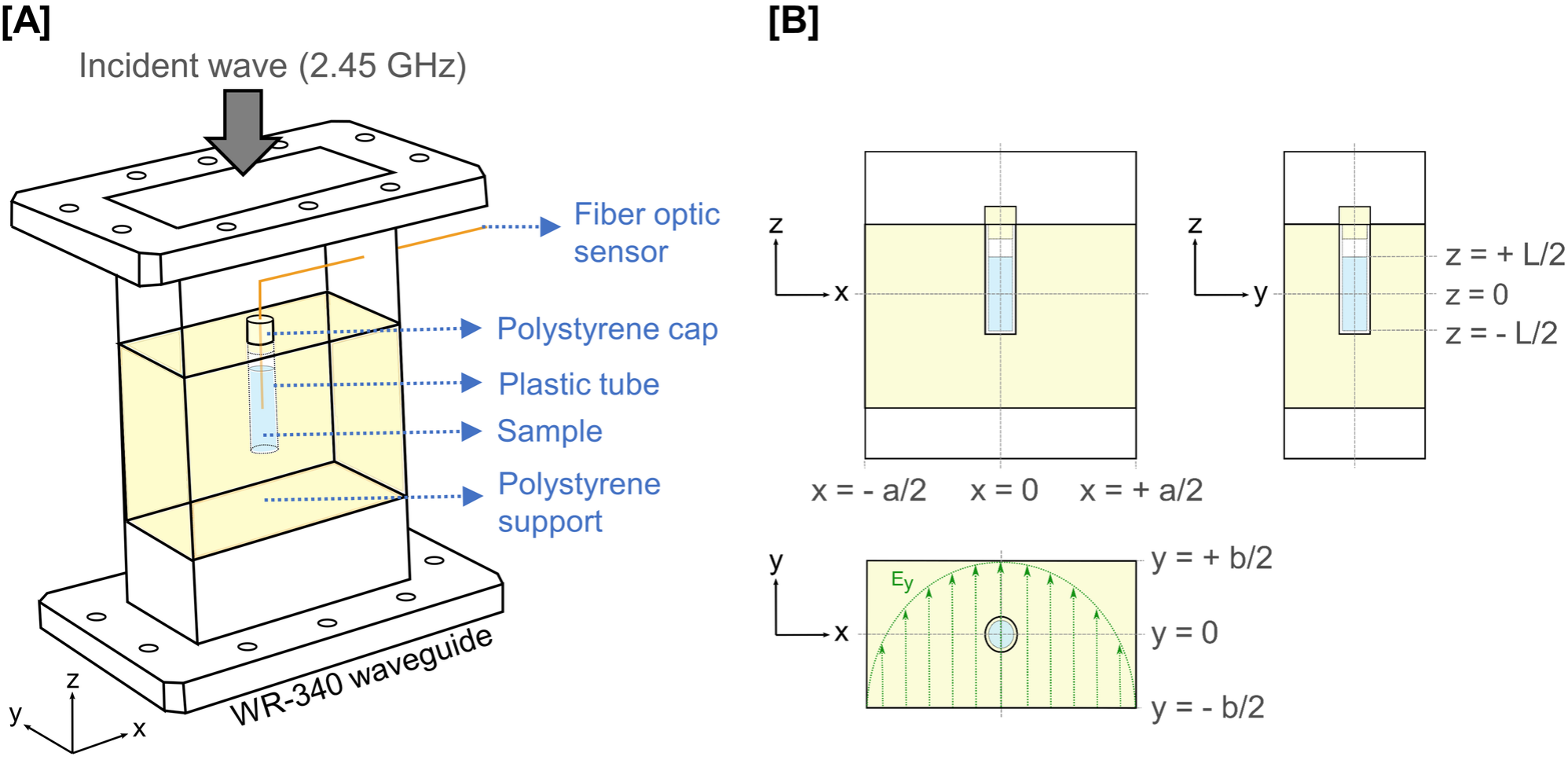

Figure 2. (A) Schematic diagram of the applicator and experimental setup for the microwave processing of fruit juice model solution. (B) Views of the arrangement of the sample, plastic tube, polystyrene cap and support inside the TE_{10} mode rectangular waveguide, where a = 86 mm, b = 43 mm, L = 24.3 mm. Electric field distribution within an empty TE_{10} waveguide in the plane xy is illustrated by dotted arrows in green.

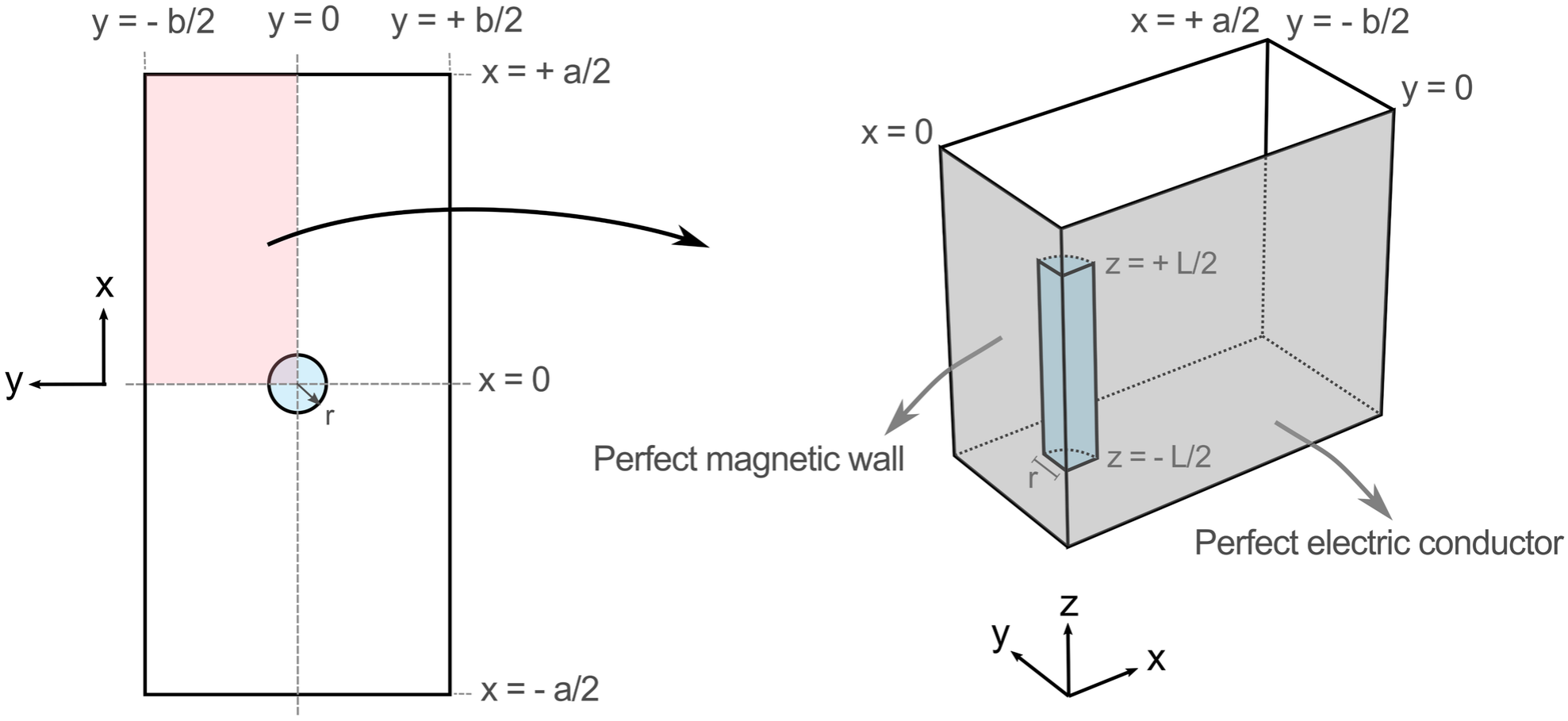

Figure 3. Model design simplification and computational domain, where a = 86 mm (x-axis), b = 43 mm (y-axis), L = 24.3 mm (z-axis) and r = 3.965 mm.

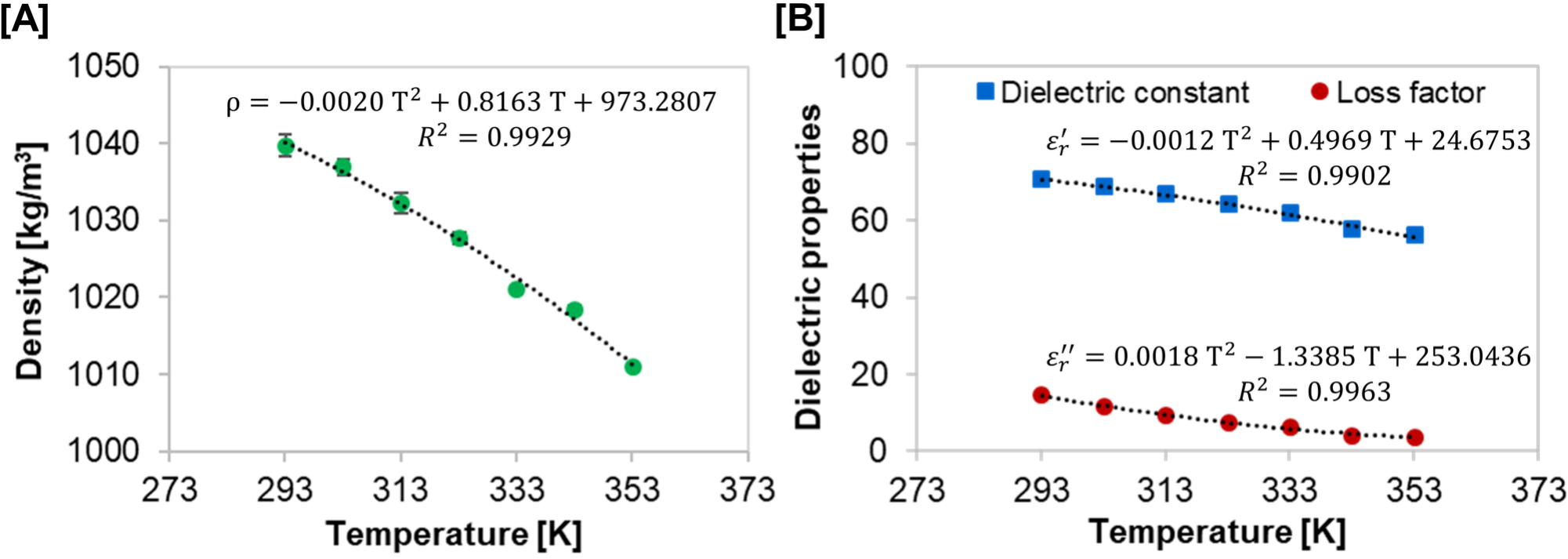

Figure 4. (A) Density and (B) dielectric constant and loss factor at 2.45 GHz of the fruit juice model solution as a function of temperature. Vertical bars indicate the standard deviation.

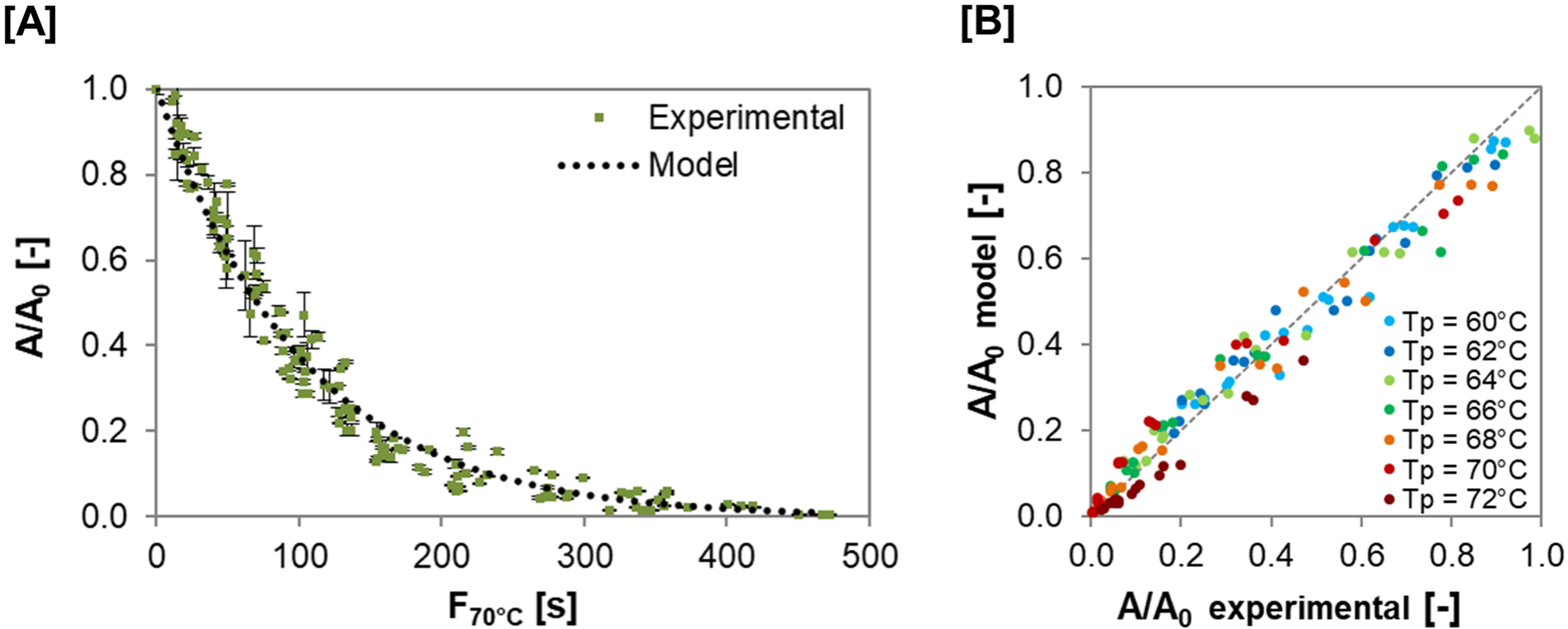

Figure 5. (A) Residual peroxidase activity (A/A_0) as a function of the equivalent time ($F_{70°C}$, considering 70 °C as the reference temperature), where green square dots are the experimental values, the vertical bars are the standard deviation and the black dotted curve is the adjusted first-order model. (B) Parity chart between the values predicted by the model and the experimental data obtained after thermal treatment at different processing temperatures (T_P).

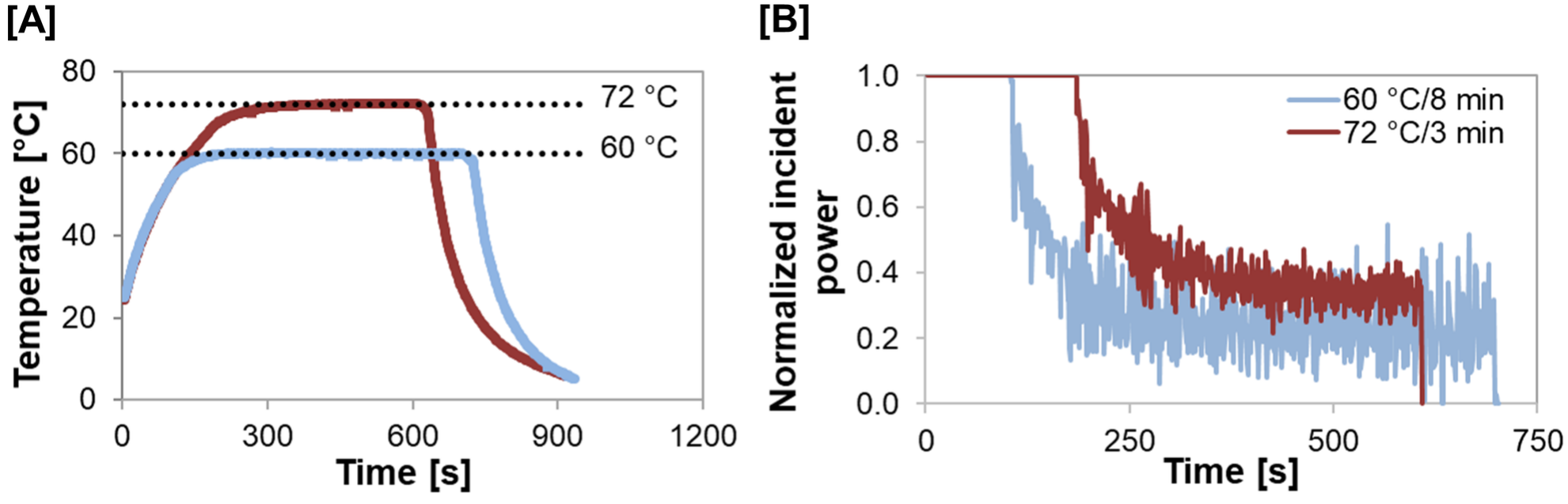

Figure 6. (A) Temperature profiles at the center of the fruit juice model solution and (B) normalized incident power along the microwave processing at the following holding temperatures and times: 60 °C for 8 min and 72 °C for 3 min.

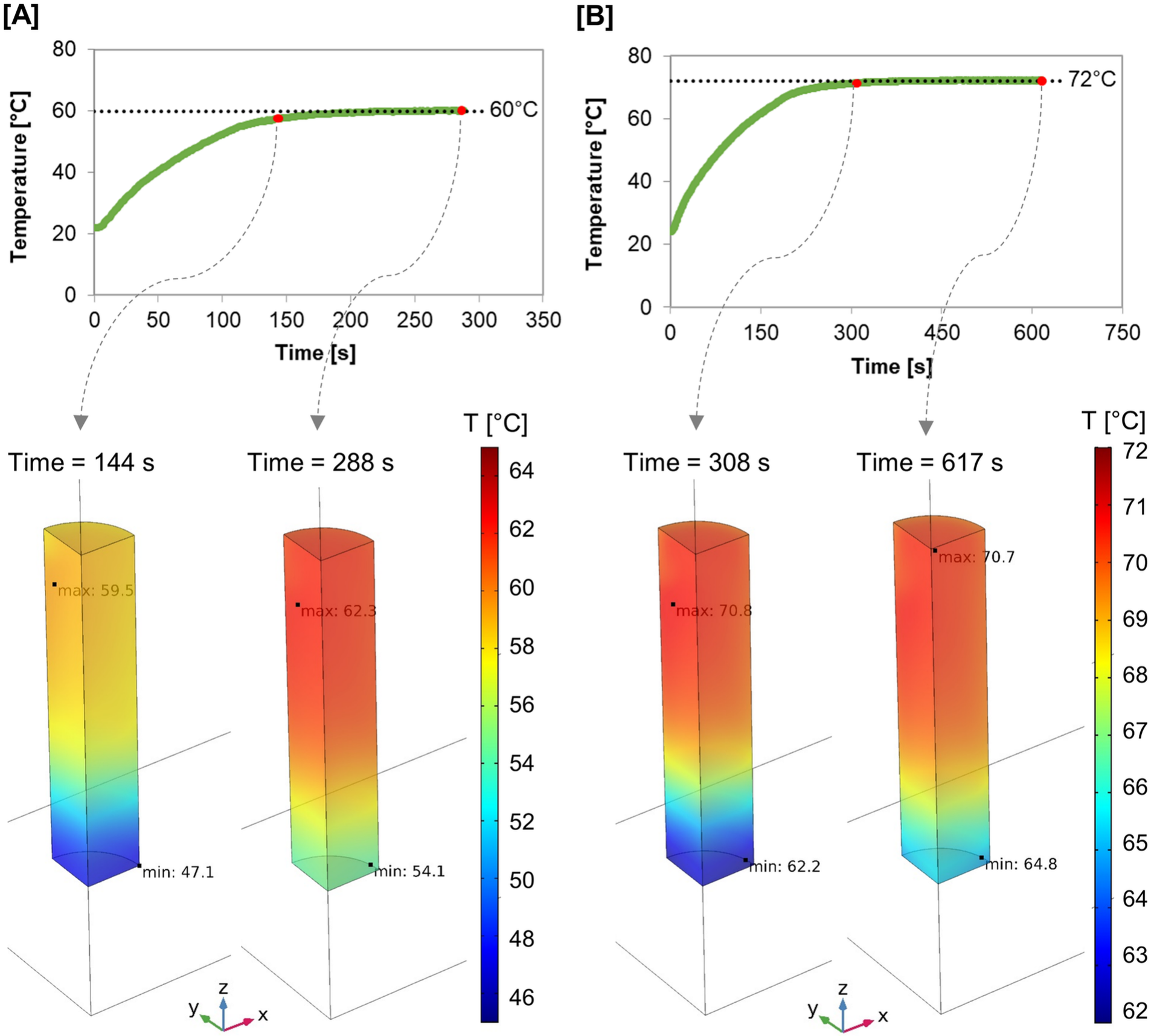

Figure 7. Temperature distribution within the sample at the middle and the end of processing times of two microwave heating conditions: (A) 60 °C/1 min and (B) 72 °C/3 min.

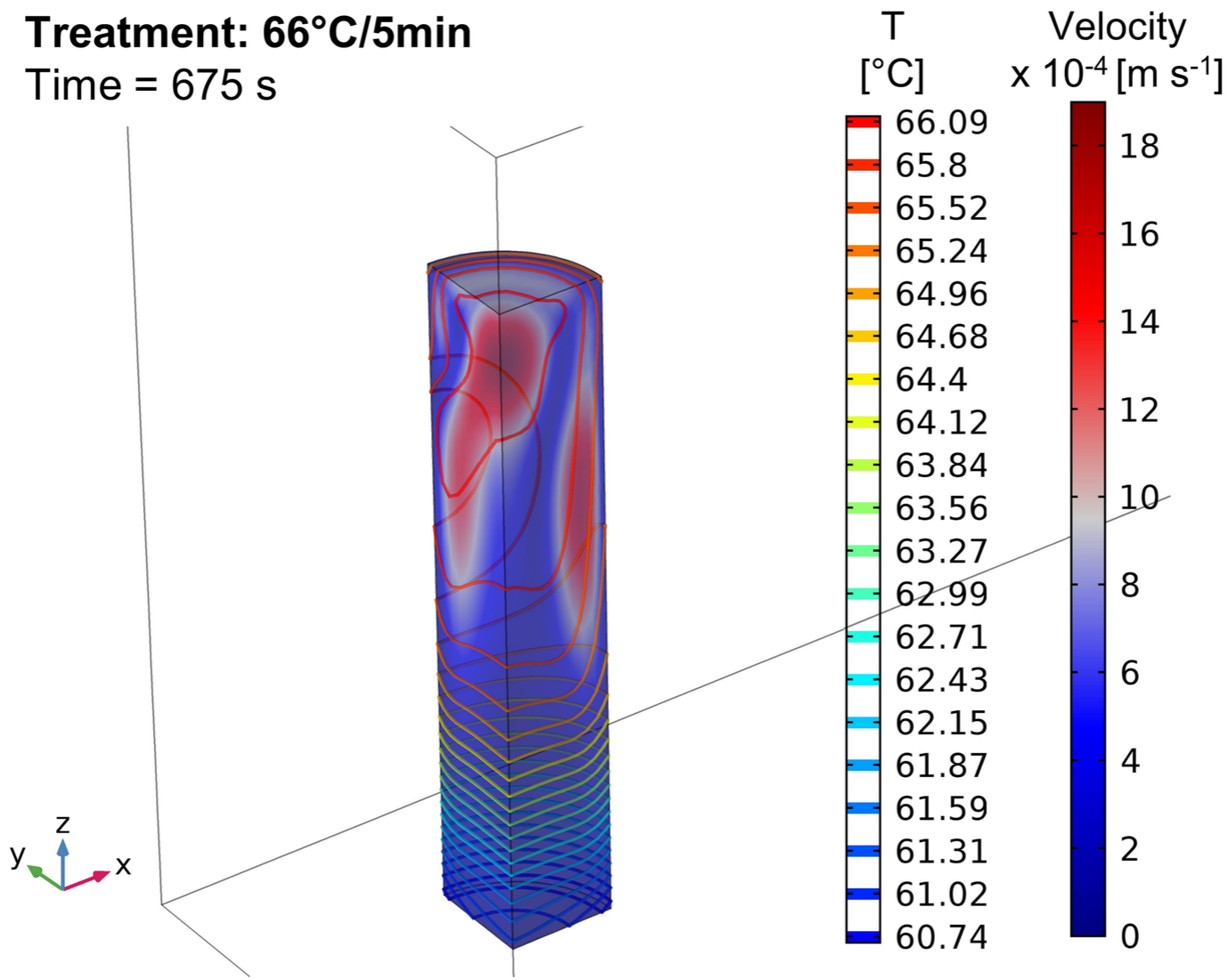

Figure 8. Distribution of temperature (contour plots) and velocity of fluid flow (volume plots) within the fruit juice model solution during the microwave treatment of 66 °C/5 min at the processing time of 675 s.

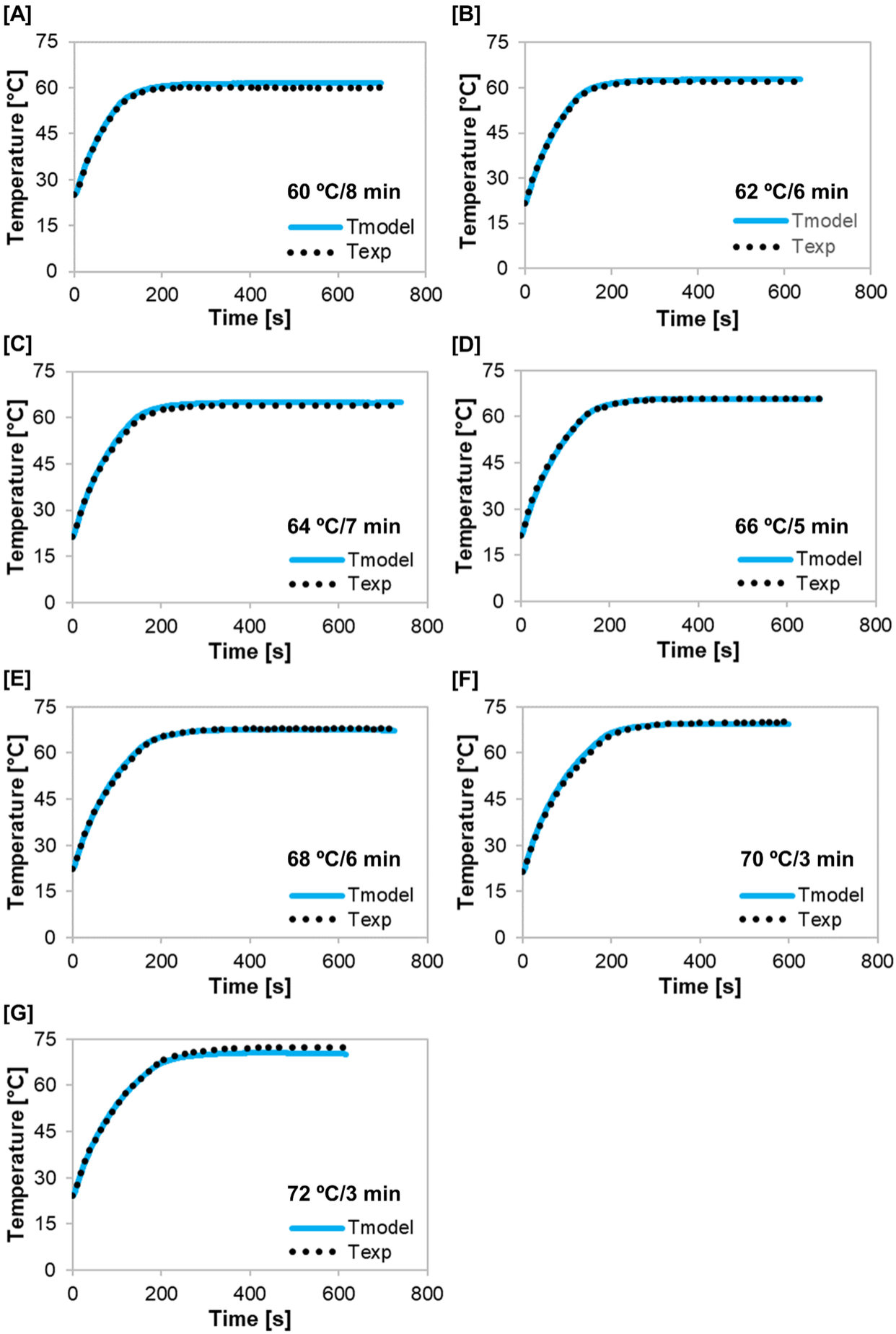

Figure 9. Predicted and experimental temperature profile at the center of the sample during the following microwave treatments: (A) 60 °C/8 min, (B) 62 °C/6 min, (C) 64 °C/7 min, (D) 66 °C/5 min, (E) 68 °C/6 min, (F) 70 °C/3 min and (G) 72 °C/3 min.

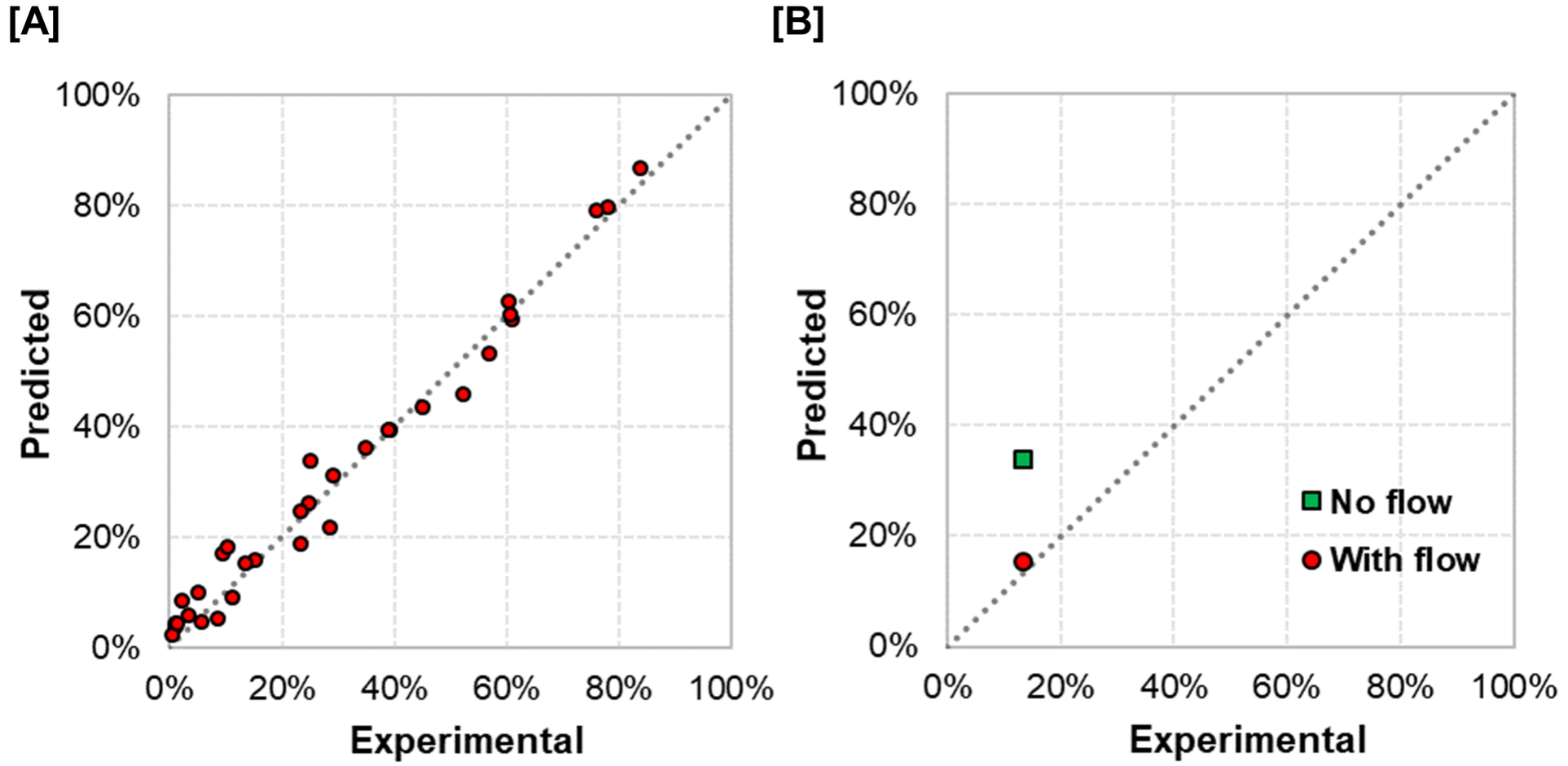

Figure 10. (A) Parity plots comparing the predicted and experimental residual peroxidase activity in fruit juice model solution after 28 different microwave treatments. (B) Parity plots comparing the predicted, considering or not fluid flow, and experimental residual peroxidase activity after the microwave treatment at 66 °C/5 min.

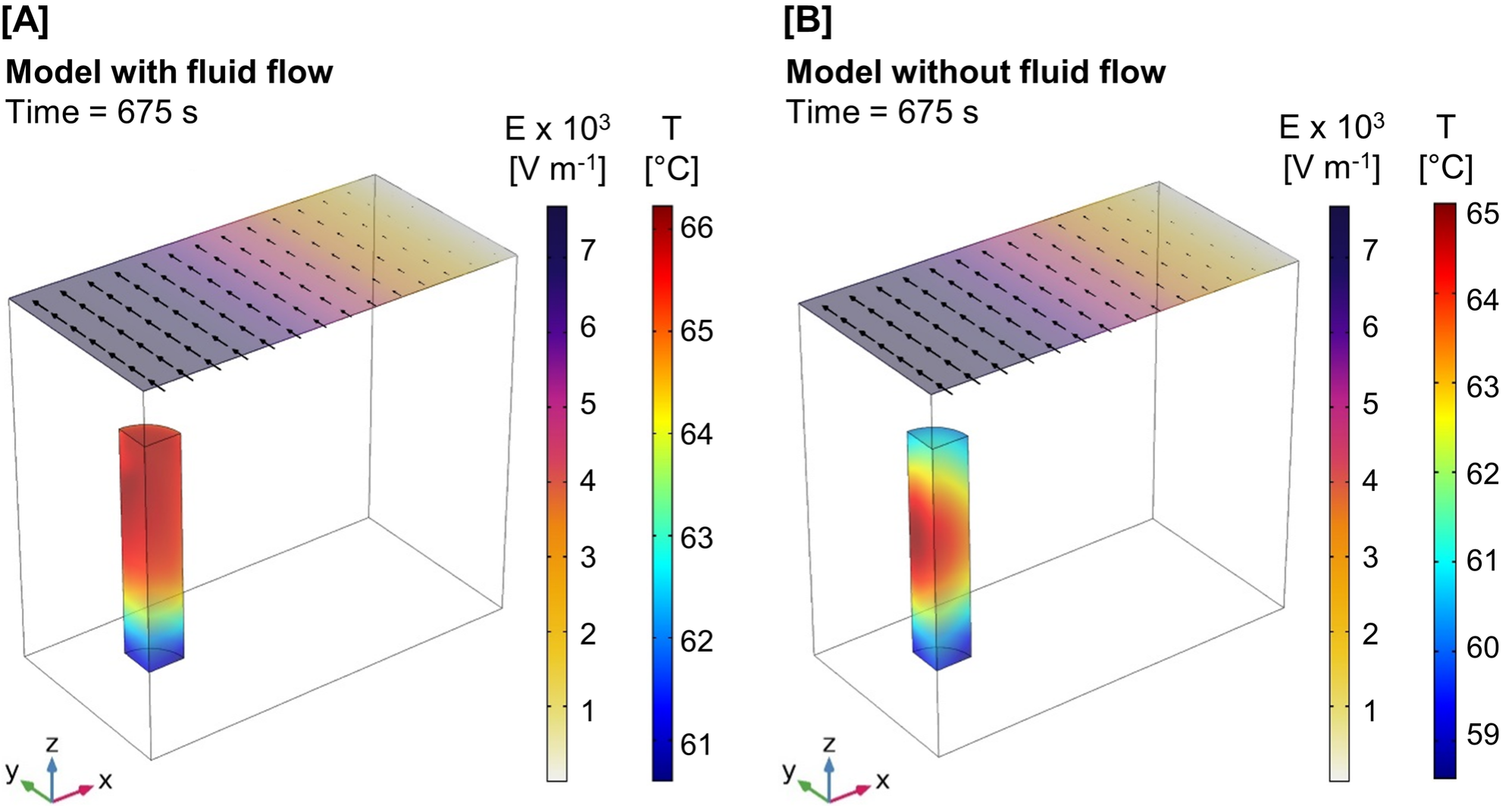

Figure 11. Temperature (T) distribution within the juice model solution and electric field (E) distribution, both at time of 675 s of a microwave treatment at 66 °C/5 min based on simulations considering fluid flow (A) and neglecting fluid flow (B).

Table 1. Equations implemented in the simulation model to describe the variation of thermophysical properties of the fruit juice model solution as a function of temperature (T in K).

Property	Equation
Thermal conductivity[1] [W m^{-1} K^{-1}]	$k = (1.208711 \cdot 10^{-3} \cdot T\ ) + (2.129341 \cdot 10^{-1})$
Heat capacity[2] [J kg^{-1} K^{-1}]	$C_p = (7.393939 \cdot 10^{-1} \cdot T) + (3.734762 \cdot 10^{3})$
Viscosity[3] [Pa s]	$\eta = (1.977074 \cdot 10^{-7} \cdot T^2) - (1.438718 \cdot 10^{-4} \cdot T) + (2.648232 \cdot 10^{-2})$
Density [kg m^{-3}]	$\rho = (-2.007069 \cdot 10^{-3} \cdot T^2) + (8.163102 \cdot 10^{-1} \cdot T) + (9.732807 \cdot 10^{2})$
Dielectric constant [-]	$\varepsilon_r^{'} = (-1.1591163420 \cdot 10^{-3} \cdot T^2) + (4.9685629334 \cdot 10^{-1} \cdot T) + (2.4675349765 \cdot 10^{1})$
Loss factor [-]	$\varepsilon_r^{''} = (1.7900147908 \cdot 10^{-3} \cdot T^2) - (1.3385095961 \cdot T) + (2.5304357446 \cdot 10^{2})$

[1] Data from Honig (1953); [2] Data from Asadi (2006); [3] Data from Telis *et al.* (2007).

Table 2. Kinetic parameters and fit criteria of the adjusted first-order kinetic model for peroxidase inactivation in fruit juice model solution by conventional heating.

Parameters		Fit criteria	
$D_{70°C}$ [s]	234.377 ± 7.068	SQE	0,223
z [°C]	12.072 ± 0.295	R^2	0,97

Table 3. Residual peroxidase activities after microwave processing at different central holding temperatures (T_H), holding times and incident energy. Mean value ± standard deviation of the process triplicate (n = 3).

T_H [°C]	Holding time [min]	Residual peroxidase activity [%]	Incident microwave energy [kJ]
60	-	84.50 ± 2.90	16.937 ± 0.123
	1	77.65 ± 1.10	19.040 ± 0.340
	4	60.92 ± 0.91	23.680 ± 0.239
	8	38.64 ± 1.25	28.816 ± 0.095
62	-	76.65 ± 1.65	19.600 ± 0.251
	2	61.80 ± 1.62	23.785 ± 0.245
	4	46.60 ± 1.45	26.768 ± 0.228
	6	34.72 ± 1.46	29.699 ± 0.262
64	-	58.90 ± 1.68	23.521 ± 0.801
	2	42.15 ± 1.01	26.001 ± 0.347
	4	25.69 ± 0.94	30.393 ± 0.246
	7	13.60 ± 1.56	35.306 ± 0.256
66	-	52.69 ± 0.60	25.139 ± 0.290
	1	39.76 ± 0.67	26.886 ± 0.341
	3	24.04 ± 0.78	31.297 ± 0.879
	5	13.97 ± 0.55	34.624 ± 0.383
68	-	24.85 ± 2.21	26.547 ± 0.089
	2	10.15 ± 0.72	30.828 ± 0.441
	4	4.89 ± 0.06	34.994 ± 0.274
	6	3.12 ± 0.36	38.181 ± 0.414
70	-	21.82 ± 3.42	31.300 ± 0.162
	1	11.39 ± 0.65	33.676 ± 0.162
	2	7.81 ± 0.75	35.968 ± 0.395
	3	5.35 ± 0.24	37.318 ± 0.059
72	-	2.05 ± 0.04	33.888 ± 0.156
	1	1.19 ± 0.26	34.738 ± 0.273
	2	1.03 ± 0.08	35.735 ± 0.694
	3	0.52 ± 0.11	38.236 ± 0.520